Ultrafast all-optical control of the magnetization in magnetic dielectrics

Andrei Kirilyuk,[a] Alexey Kimel, Fredrik Hansteen, and Theo Rasing

IMM, Radboud University Nijmegen, Toernooiveld 1, 6525 ED Nijmegen, The Netherlands

Roman V. Pisarev

Ioffe Physico-Technical Institute, 194021 St. Petersburg, Russia
(Submitted February 24, 2006)
Fiz. Nizk. Temp. **32**, 985–1009 (August-September 2006)

The purpose of this review is to summarize the recent progress on laser-induced magnetization dynamics in magnetic dielectrics. Due to the slow phonon-magnon interaction in these materials, direct thermal effects of the laser excitation can only be seen on the time scale of almost a nanosecond and thus are clearly distinguished from the ultrafast nonthermal effects. However, laser pulses are shown to indirectly modify the magnetic anisotropy in rare-earth orthoferrites via the crystal field, and to bring about spin reorientation within a few picoseconds. More interesting, however, are the direct nonthermal effects of light on spin systems. We demonstrate coherent optical control of the magnetization in ferrimagnetic garnet films on a femtosecond time scale through a combination of two different ultrafast and nonthermal photomagnetic effects and by employing multiple pump pulses. Linearly polarized laser pulses are shown to create a long-lived modification of the magnetocrystalline anisotropy via optically induced electron transfer between nonequivalent ion sites. In addition, circularly polarized pulses are shown to act as strong transient magnetic field pulses originating from the nonabsorptive inverse Faraday effect. An all-optical scheme of excitation and detection of different antiferromagnetic resonance modes with frequencies of up to 500 GHz will be discussed as well. The reported effects open new and exciting possibilities for ultrafast manipulation of spins by light and provide new insight into the physics of magnetism on ultrafast time scales.
[DOI: 10.1063/1.2219497]

I. INTRODUCTION

Ultrafast magnetization dynamics has attracted lively interest in recent years,[1–10] stimulated, on the one hand, by the demand for increased speed of writing and retrieving magnetically stored information, and, on the other hand, by the development of ultrafast (femtosecond) laser sources.[11] Such lasers allow for excitation of magnetic systems at much shorter time scales than fundamental quantities such as spin precession or spin-lattice relaxation times. This type of photoexcitation brings a medium to a strongly nonequilibrium state, where a conventional description of magnetic phenomena in terms of thermodynamics may no longer be valid. Therefore, in addition to the potential applications, ultrafast magnetization dynamics is a subject of extreme fundamental interest in the physics of magnetism.

The first ultrafast time-resolved studies of the impact of laser pulses on the magnetization were done on Ni and Fe using picosecond laser pulses, but these were not successful in observing any magnetic effects up to the melting point of the samples.[12,13] Later, using time-resolved spin-polarized photoemission as a probe of the magnetization, Vaterlaus *et al.*[14] succeeded in estimating the spin-lattice relaxation time in Gd films to be (100±80) ps. In 1996 Beaurepaire *et al.*[1] reported the first observation of subpicosecond demagnetization in Ni induced by 60-fs laser pulses. This ultrafast magnetic response was explained by an effetive electron-spin interaction mechanism among the strongly nonequilibrium photoexcited electrons, leading to a rapid increase of the spin temperature and destruction of the magnetization. The observation triggered the interest of several groups, and similar experiments confirmed the ultrafast demagnetization in Ni, Co, and other metallic systems.[15–18] It was concluded that the magnetization follows the electron temperature with a possible delay between the electron excitation and the magnetic breakdown of no more than 50 fs. An experimental artifact was revealed by Regensburger *et al.*[19] and Koopmans *et al.*,[20] who pointed out that the magnetooptical response does not always directly relate to the magnetization during the first few hundred femtoseconds as a result of hot-electron effects. The speed of the true demagnetization was consequently reduced to 0.5–1 ps and ascribed to an effective spin-lattice interaction. The significant role of possible artifacts in time-resolved magnetooptical experiments was also demonstrated in *ab initio* calculations.[21] Recently, however, it was shown that laser-induced spin dynamics indeed does take place during the initial electron thermalization, with a characteristic time of about 50 fs,[22–24] thus again raising the question of the underlying mechanism. The complete interpretation of this rapid demagnetization is still not clear, partly because it is difficult to distinguish between different processes in metallic systems due to their complex electronic structure and the continuum of transitions.[21,25,26]

In addition to laser-induced demagnetization, the triggering of spin waves by laser pulses has been studied.[27–32] The equilibrium orientation for the magnetization is believed to be changed through thermal modulation of the magnetic anisotropy (that includes shape anisotropy), which causes the

magnetization to precess. In fact, for all of the above-mentioned experiments on metallic systems, the observed magnetic excitation was the result of optical absorption followed by a rapid temperature increase. Far more exciting is the possibility of ultrafast *nonthermal* control of magnetization by light, where a change in the magnetization is not simply the result of a temperature increase. It provides much greater freedom for the manipulation of the magnetization, and unwanted heating and possible material damage in devices can be avoided. The nonthermal influence of light on magnetization in metals has been predicted by theory,[33] but many aspects of this are still subject to debate.[21] A few experimental attempts to observe a nonthermal influence of light on metallic magnetic systems have been reported.[31,34] However, no impact on the magnetization could be seen in the time after the optical pulse. We believe that this is partly due to the dominating thermal effect in metals, and to the unfortunate coincidence of several processes in the same narrow time window, which hampers the analysis.[35,36]

Recently, a lot of attention has been attracted to novel ferromagnetic semiconducting compounds.[37,38] In this type of material the ferromagnetism is mediated by the free carriers, and highly effective nonthermal control of the magnetization by light has been reported from static measurements.[39] However, these large values of the photoinduced magnetization have not been reproduced or confirmed by dynamic measurements with subpicosecond time resolution,[40,41] and similar experiments have only shown the thermal effects of light on the magnetic system.[42,43] A number of difficulties are associated with this relatively new class of materials, and the understanding of their electronic, optical, and magnetic properties is currently very limited and controversial.

When seeking to improve our understanding of ultrafast spin dynamics and searching for nonthermal photomagnetic effects, dielectrics possess some significant advantages over metals and semiconductors. The phonon-magnon interaction responsible for thermal effects is much slower in dielectrics than in metals and does therefore not obscure the interpretation of the processes on shorter time scales.[44] Moreover, the electron-spin scattering mechanism proposed in metals cannot exist in dielectrics due to the localized nature of their electronic states. And, finally, magnetic dielectrics, in contrast to the novel magnetic semiconductors, are characterized by a well-defined electronic structure, and their optical and magnetic properties are well understood.

Magnetic garnets have been for a long time one of the most popular types of magnetic dielectric materials for both research and applications.[45,46] Their physical properties are well known and can be tailored over a wide range through chemical substitution and by varying their growth conditions. For decades they have been considered ideal model systems for the experimental and theoretical investigation of magnetic phenomena. Their optical absorption in the infrared spectral region is very low, and they exhibit large magnetooptical effects caused by strong spin-orbit coupling. The linewidth of ferrimagnetic resonance in garnets can be extremely narrow, implying a very low damping of magnetic excitations.[45] Additionally, static control of the magnetic anisotropy by light has been known for some time in this class of materials.[47,48] For these reasons they seem to be ideal materials for the study of ultrafast spin dynamics in general and the search for nonthermal mechanisms for the optical control of magnetization in particular.[49–51]

Another interesting group of dielectrics, the rare-earth orthoferrites $RFeO_3$, are also a well-studied family of magnetic materials with a rich array of magnetic properties.[52] The orthoferrites are particularly interesting because of the presence of an antisymmetric exchange interaction which involves the vector (cross) product of neighboring spins as opposed to the usual scalar product. In the absence of this interaction, the orthoferrites would be antiferromagnetic. Its presence leads to a small canting of the sublattices, making the orthoferrites "weak" ferromagnets with $4\pi M_s \simeq 100$ G. Another interesting feature of these materials is the fact that some of them exhibit a transition as a function of temperature, in which the direction of the antiferromagnetically ordered spins and consequently also of the net magnetization rotates by 90°. The combination of high magnetic resonance frequencies with very large magnetooptical effects makes the orthoferrites interesting objects for study of laser-induced dynamics.[9,10]

The purpose of this paper is to summarize the results from our recent extensive studies of ultrafast optical control of the magnetization in both ferrimagnetic garnet films and in weakly ferromagnetic orthoferrites. Laser pulses of center wavelength $\lambda = 805$ nm and pulse width of about 100 fs were used to both excite and probe the magnetic response of the samples. We demonstrate the existence of different nonthermal photo- and optomagnetic effects, allowing for ultrafast control of both the magnetocrystalline anisotropy and the magnetization. Note that optomagnetic effects differ from the photomagnetic ones by the fact that the former are unrelated to the absorption of the light and can be seen most obviously in transparent crystals.[49,53] The light wave is then equivalent to an effective magnetic field. In the latter case the light, as it absorbed, excites electrons into localized energy levels. Such a redistribution of electron density causes changes in the properties of the spin system, e.g., changes in the anisotropy constants. Thermal effects can be clearly distinguished from these nonthermal effects and are observed on the time scale of several hundreds of picoseconds in the vicinity of the Curie temperature, which is demonstrated in iron borate $FeBO_3$.

The paper is organized as follows: Experimental details including sample characteristics, experimental setup, and principles of magnetic precession as the measured quantity are given in Sec. II. Section III A introduces the time scale of phonon-magnon relaxation responsible for the thermal quenching of magnetization. Then, Secs. III B and III C deal with direct nonthermal excitation of the magnetization dynamics on a femtosecond time scale via the inverse Faraday effect. In Sec. IV we present and discuss the magnetization dynamics obtained via laser-induced modification of magnetic anisotropy, via thermal (Sec. IV A) and nonthermal (Sec. IV B) mechanisms. Finally, in Sec. V we demonstrate how a combination of two pump pulses and/or different nonthermal effects can lead to coherent control of magnetization dynamics, and illustrate this by the example of single-pulse ultrafast photomagnetic switching.

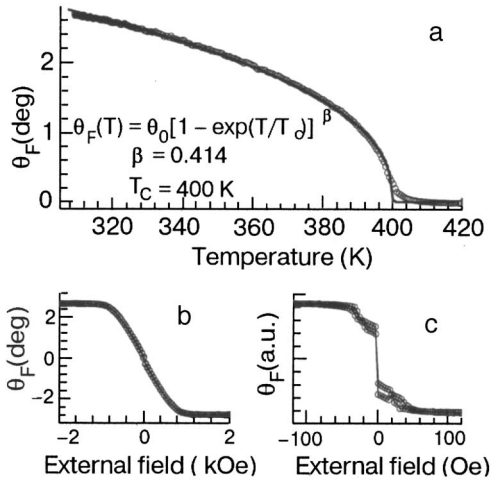

FIG. 1. Garnet sample characteristics: (a) Measured Faraday rotation θ_F at $\lambda = 805$ nm as a function of temperature with a saturating applied field $\mathbf{H}_{ext}$ normal to the film plane. (b) Hysteresis loop at $T = 300$ K measured with $\mathbf{H}_{ext}$ normal to the film. (c) Hysteresis loop measured at a small angle of incidence with $\mathbf{H}_{ext}$ in the sample plane, indicating the presence of anisotropy fields of about 50 Oe.[51]

II. EXPERIMENTAL METHODS

A. Samples

1. Magnetic garnets

The ferrimagnetic garnet samples studied in this work are 4–8 μm thick ferrimagnetic garnet films of the composition $Lu_{3-x-y}Y_xBi_yFe_{5-z}Ga_zO_{12}$ grown on (001) oriented gallium gadolinium garnet (GGG) substrates by liquid phase epitaxy. All the results mentioned in this review are from samples with $x = 0.65$, $y = 0.66$, and $z = 1.15$, but the effects that we observe are also present in a whole series of samples with similar composition. Small amounts of Pb impurities are known to exist in these types of films due to the flux from which they are grown. The films have in-plane magnetization $4\pi M_s = 550$ G and Curie temperature $T_C = 400$ K. While bulk garnet crystals have cubic symmetry and possess a center of inversion, epitaxially grown thin garnet films seem to lack this center of symmetry, as has been demonstrated by the existence of a linear magnetoelectric effect[54] and by strong optical second-harmonic generation.[55,56]

The linear optical absorption of these garnet films in the spectral region around $\lambda = 805$ nm (1.54 eV) is small ($\alpha \equiv 20$ cm^{-1}) and mainly due to spin- and parity-"forbidden" *d-d* transitions in the Fe^{3+} ions and a tail from higher-energy charge-transfer transitions at 2.8 and 3.4 eV.[45,46] The magnetooptical properties of the material in the infrared part of the spectrum are dictated mainly by the tails of these high energy transitions. It is also well known that bismuth substitution strongly enhances the magnetooptical response.[45,46]

The Faraday rotation θ_F measured with a saturating external field normal to the film plane is shown as function of the sample temperature in Fig. 1a for a 7.5-μm thick garnet film. $M(T)$ exhibits a second-order phase transition with a critical exponent $\beta = 0.414$ and a Curie temperature of $T_C = 400$ K, both in agreement with previous studies of similar materials.[45,46] From the hysteresis loop in Fig. 1b it can be seen that the sample exhibits no coercivity and has a large Faraday rotation of about 2.5° at room temperature when saturated in the out-of-plane direction. The Faraday rotation measured at a small angle of incidence with the applied magnetic field parallel to the sample plane is shown by the hysteresis loop in Fig. 1c. It gives an estimate of the film in-plane anisotropy H_a of about 50 Oe. Vibrating sample magnetometer (VSM) measurements reveal that this anisotropy has a fourfold symmetry in the plane.

2. Rare-earth orthoferrites

Another class of dielectric magnetic materials is comprised of the antiferromagnetic rare-earth orthoferrites $RFeO_3$, where R is a rare-earth ion, Dy or Tm in this paper. These materials crystallize in an orthorhombically distorted perovskite structure, with a symmetry space group D_{2h}^{16} ($Pbnm$).[52,57] The iron moments order antiferromagnetically, but with a small canting of the spins on different sublattices. The spins of the dysprosium and thulium ions are not ordered above 4 K, being in a paramagnetic state. The spins of the Fe^{3+} ions ($3d^5$, ground state $^6A_{1g}$, $S = 5/2$) are coupled antiferromagnetically by isotropic exchange. The Dzyaloshinskii-Moriya interaction[58,59] leads to a slight canting of opposite spins with an angle of about 0.5°, giving rise to a spontaneous magnetization $M_s \sim 8$ G. Despite the small magnetization, this material exhibits a giant Faraday rotation of about 3000° cm^{-1} owing to its strong spin-orbit interaction.[60]

The $TmFeO_3$ and $DyFeO_3$ single crystals used in our experiments were grown by the floating-zone method under optical heating.[61] The crystals were oriented by x-ray diffractometry. Since orthoferrites are optically biaxial crystals, the samples were prepared in the form of platelets polished down to a thickness of 60–100 μm, with the surface normal oriented perpendicular to the *x*, *y*, or *z* crystallographic axes to within a few degrees, as well as of platelets with the normal approximately aligned with the optical axis lying in the *yz* plane.

Rare-earth orthoferrites are optically biaxial crystals possessing inherent birefringence. Therefore, the polarization state of light propagating through these crystals changes. We measured the phase difference between the two orthogonal polarization components of light transmitted through a sample for each wavelength in the case where light is incident normal to the sample and is linearly polarized at 45° to the crystallographic axes.

Several orthoferrites are known for a strong temperature-dependent anisotropy.[52,57] Thus, as the temperature is lowered, spontaneous spin reorientation occurs in $TmFeO_3$ as a result of variation of the magnetic anisotropy. In this process, the ferromagnetic moment turns continuously from its position along the *z* axis at a temperature T_2 to the position along the *x* axis at a temperature T_1 (see Fig. 2a). These points are the temperatures of second-order phase transitions ($\Gamma_4 \rightarrow \Gamma_{24} \rightarrow \Gamma_2$)[62] in which anomalies of the physical properties are observed.

The temperature dependence of the linear birefringence is plotted in Fig. 2b and is indeed seen to exhibit two second-order orientational phase transitions at temperatures of 83 and 93 K. Below, in Sec. III A we will show how such transitions can be triggered by a laser pulse on a time scale of a few picoseconds.

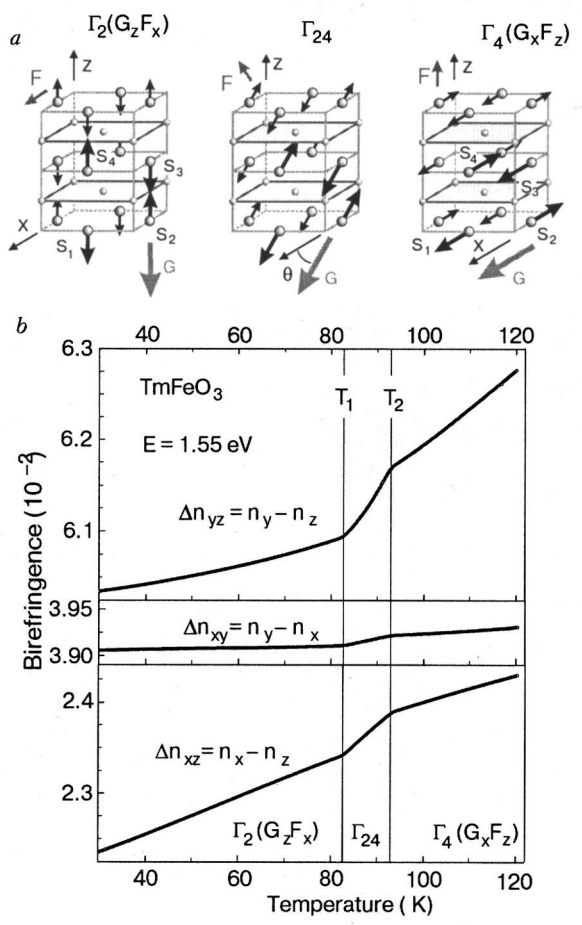

FIG. 2. (a) Crystallographic and spin structure of $TmFeO_3$ showing different phases as well as the reorientation of the ferromagnetic $F=S_1+S_2+S_3+S_4$ and antiferromagnetic $G=S_1-S_2+S_3-S_4$ vectors. (b) Temperature dependence of the birefringence along the three principal crystallographic directions. The birefringence anomalies occur at the orientational-transition temperatures T_1 and T_2.[63]

The other orthoferrite considered, $DyFeO_3$, has properties similar to those of $TmFeO_3$ except for another type of phase transition that occurs at a lower temperature. This transition, however, is of no concern for this review.

3. Iron borate $FeBO_3$

Iron borate crystallizes in a calcite type structure with space group $R\bar{3}c$ and has a Néel temperature $T_N \approx 348$ K. Similar to the orthoferrites, the antiferromagnetic state of $FeBO_3$ is characterized by a weak ferromagnetism due to a slight spin canting of about 1 degree in the (001) plane, which results in a magnetic moment oriented within this plane. Due to this magnetic moment one can turn the $FeBO_3$ sample into a single-domain state with the help of a small magnetic field, and linear magnetooptical effects can be used to probe the antiferromagnetic ordering. Moreover, $FeBO_3$ has its Néel point slightly above room temperature and is characterized by good transparency in the visible spectral range. Therefore this compound is both convenient for study and suitable for potential applications.

The optical properties of $FeBO_3$ are determined by the *d-d* transitions in the partially filled *d* shell of the Fe^{3+} ion. Figure 3 shows the relevant part of the electronic energy

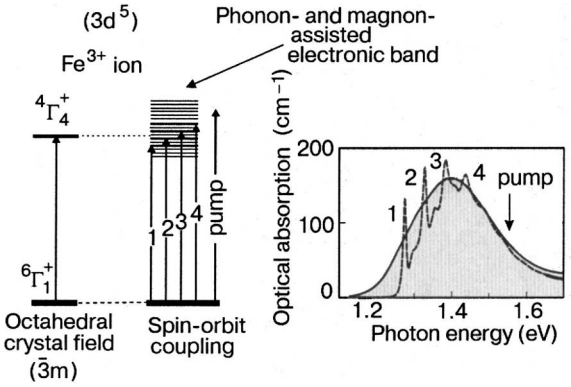

FIG. 3. The energy level scheme and the absorption spectra of $FeBO_3$ at room temperature (solid line) and at 20 K (dashed line). The spectral lines from 1 to 4 correspond to the transitions from the ground state $^6\Gamma_1^+$ to the excited state $^4\Gamma_4^+$ split by the spin-orbit coupling.[44]

diagram as derived from the local symmetry of the Fe^{3+} ion. In the crystalline field, the $3d5$ electrons of Fe^{3+} ions occupy the ground state $^6\Gamma_1^+$ ($S=5/2$), which is an orbital singlet and the only spin sextet state. The lowest excited state is triplet $^4\Gamma_4^+$ ($S=3/2$). The spin degeneracy is lifted due to the spin-orbit coupling and the exchange interaction.

The transition $^6\Gamma_1^+ \rightarrow {}^4\Gamma_4^+$ is centered at 1.4 eV and is forbidden in the electric dipole approximation because of the selection rules imposed on parity and spin. Nevertheless, from the absorption spectra measured at 20 K four intensive spectral lines were distinguished near the first *d-d* transition (see Fig. 3). At higher temperatures the splitting is not seen because of increased electron-phonon interaction and phonon-assisted transitions.

The sample was a plate of thickness 300 μm, oriented with its plane perpendicular to the hard magnetic axis.

B. All-optical pump-probe measurements

The samples were studied in transmission using an all-optical pump and probe technique. Regeneratively amplified 100 fs pulses of wavelength $\lambda=805$ nm emitted from a Ti-:sapphire laser system at a repetition rate of 1 kHz were split into two parts using a beam splitter. The most intense part (pump) was incident on the sample at near normal incidence. The magnetization dynamics induced by these pump pulses was followed in time by measuring the Faraday rotation θ_F of the time-delayed and much weaker probe pulses ($I_{\text{pump}}/I_{\text{probe}} > 100$) as function of the variable pump-probe time delay Δt. The Faraday angle θ_F is proportional to the projection of the magnetization vector $\mathbf{M}$ along the wave vector $\mathbf{k}$ of the probe light:

$$\theta_F \propto \mathbf{M} \cdot \mathbf{k}. \tag{1}$$

In our geometry (see Fig. 4) the measured Faraday rotation is therefore essentially a probe of the out-of-plane M_z component of the magnetization. For sensitive detection of the magnetooptical Faraday rotation a balanced photodiode detector was used in combination with a BOXCAR integrator.[64] A synchronized optical chopper operating at 500 Hz was placed in the pump beam path, thereby blocking every second pump pulse and creating alternating pump-on and pump-off conditions in the sample. For every pump-

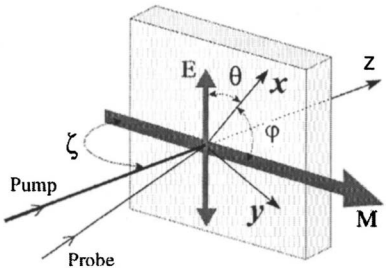

FIG. 4. Experimental geometry. Pump and probe pulses were incident on the garnet film at near normal incidence. The magnetization **M** of the sample forms an angle ζ with the sample normal [001] and an angle φ with the crystallographic [100] x axis of the film. For linearly polarized pump pulses the angle of the electric field component **E** of the light with respect to the sample x axis is denoted θ.

probe delay Δt the pump-induced Faraday rotation was averaged over several excitation events by use of a lock-in amplifier. Pump-induced changes of the optical transmittivity of the sample were recorded simultaneously with the Faraday rotation, by measuring the intensity of the probe pulses in addition to their polarization rotation.

In some cases, for example in orthoferrites in the absence of an external magnetic field, it was preferable to use the linear magnetic birefringence as a probe for the magnetic order. Such probe is insensitive to the presence of 180° magnetic domains and gives a direct indication of the dynamics of antiferromagnetic order.

Pump pulses of energy up to 20 μJ were focused to a spot diameter of about 200 μm on the sample, corresponding to a photon density of approximately one photon per unit cell in the irradiated sample volume. The laser peak power density of about 10^{11} W/cm^2 is still well below the threshold for continuum generation in the garnet films. While the probe pulses always were linearly polarized, the polarization of the pump pulses could be varied using a Babinet-Soleil compensator. A magnetic field was applied either in the xy plane of the sample, see Fig. 4, or at an angle with respect to the sample normal, thereby pulling the magnetization **M** out of the film plane ($\zeta < 90°$). The sample temperature could be controlled from room temperature up to well above the Curie point using a sample holder with a built-in heater and an electronic temperature regulator. Alternatively, the sample could be cooled down to about 5 K by using an optical flow cryostat, where the temperature was stabilized better than 0.5 K.

C. Magnetic precession as a key process

In the following Sections we present, interpret, and discuss our experimental results from extensive studies of optically induced magnetization dynamics in garnet films and orthoferrite single crystals. A remarkable amount of information about the underlying photomagnetic mechanisms can be obtained simply by analyzing time-traces of the precessional dynamics.

Coherent precession is the fastest known way to alter the direction of the macroscopic magnetization in a material. Phenomenologically the process is described by the Landau-Lifshitz equation of motion,[65,66]

$$\frac{d\mathbf{M}}{dt} = -\gamma(\mathbf{M} \times \mathbf{H}_{\text{eff}}). \tag{2}$$

It follows from this that the equilibrium orientation ($d\mathbf{M}/dt = 0$) for the magnetization **M** is along the direction of the effective magnetic field $\mathbf{H}_{\text{eff}}$, which is composed of the externally applied field $\mathbf{H}_{\text{ext}}$, the anisotropy field $\mathbf{H}_{\text{an}}$, and the demagnetizing field $\mathbf{H}_{\text{dem}} = 4\pi M_z$:

$$\mathbf{H}_{\text{eff}} = \mathbf{H}_{\text{ext}} + \mathbf{H}_{\text{an}} + \mathbf{H}_{\text{dem}}. \tag{3}$$

The key to optical manipulation of the magnetization lies in the control of these fields by light. The description of spin dynamics in orthoferrites is only slightly more complicated because of the antiferromagnetic character of the exchange coupling. The equilibrium orientation of the spins in this material is given by the minimum of the thermodynamic potential Φ (Ref. 52):

$$\Phi = J(\mathbf{S}_1 \cdot \mathbf{S}_2) + \mathbf{D} \cdot [\mathbf{S}_1 \times \mathbf{S}_2] + K_x(S_{1x}^2 + S_{2x}^2) + K_z(S_{1z}^2 + S_{2z}^2) + K_4(S_{1x}^4 + S_{1y}^4 + S_{1z}^4 + S_{2x}^4 + S_{2y}^4 + S_{2z}^4) + \mathbf{H}(\mathbf{S}_1 + \mathbf{S}_2), \tag{4}$$

where $\mathbf{S}_1$ and $\mathbf{S}_2$ are the vectors that characterize the spins of the iron ions in the two magnetic sublattices, J is the nearest-neighbor isotropic exchange interaction constant; D is the Dzyaloshinskii-Moriya antisymmetric exchange constant; K_x, K_z, K_4 are magnetocrystalline anisotropy constants, and **H** is the external magnetic field. The constant J favors an antiferromagnetic configuration of the Fe^{3+} spins, whereas the constant of the antisymmetric exchange interaction D results in a slight canting of the spins from the antiparallel orientation over an angle $\beta \sim 0.5°$, so that the system acquires a weak ferromagnetic moment.

The resulting equations of motion for the antiferromagnetic spins $\mathbf{S}_1$ and $\mathbf{S}_2$ show that two different resonance modes can exist, with the energies:[52,57,67,68]

$$\hbar\omega_{FM} = \sqrt{24JS(K_x - K_z)S}, \tag{5}$$

$$\hbar\omega_{FM} = \sqrt{24JS(6DS\tan\beta + K_xS)}. \tag{6}$$

The first, "quasi-ferromagnetic" mode softens in the spin-reorientation region, where the modulus $|K_x - K_z|$ vanishes. The second, "quasi-antiferromagnetic" mode is usually characterized by a weaker temperature dependence. The motion of spins corresponding to these modes is discussed below, in Sec. III C and Fig. 13, where it is also shown how these modes can be excited and observed in an all-optical scheme.

Below we describe and discuss different photomagnetic effects that have been found to trigger coherent precession of the magnetization. Thus, Sec. III A describes thermally induced quenching of magnetization in $FeBO_3$ via the phonon-magnon relaxation mechanism. In Secs. III B and III C an ultrafast nonthermal effect of circularly polarized laser pulses on the magnetization is discussed along with experimental results on both garnet and orthoferrite samples. It is found that these pulses act as strong axial magnetic field pulses during their presence in the sample. The effect, also called inverse Faraday effect, is practically instantaneous and causes the magnetization to start precessing immediately after the photoexcitation. Next, in Sec. IV A we demonstrate that spin reorientation can be achieved on a picosecond time

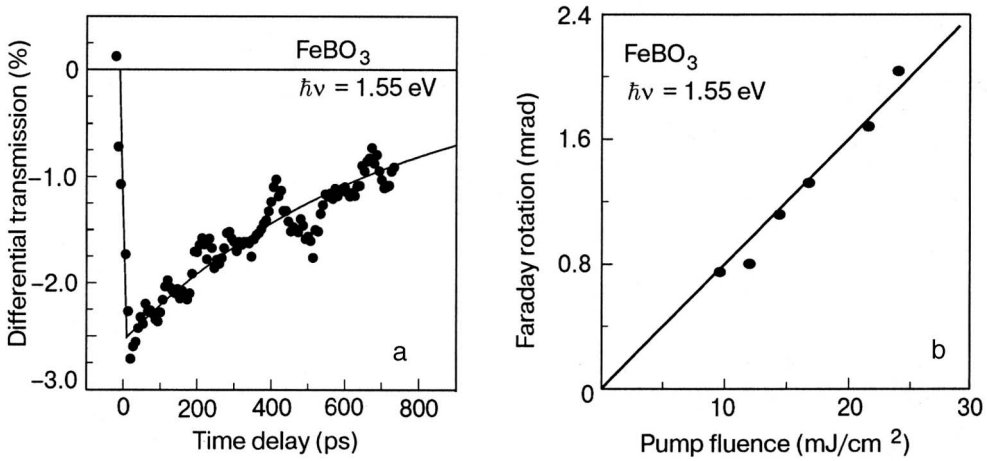

FIG. 5. (a) The transmission as a function of time delay, (b) the intensity dependence of the ultrafast Faraday rotation (symbols); linear fit with a slope of $(8\pm0.6)\cdot10^{-5}$ rad·cm^2/mJ (line).[44]

scale via ultrafast thermal modification of the anisotropy axis in $TmFeO_3$. Further, in Sec. IV B we present results showing that linearly polarized laser pulses create a long-lived modification of the magnetocrystalline anisotropy in garnet films. This latter effect is of nonthermal origin, even though it relies on absorption, unlike the inverse Faraday effect. Using a two-pulse excitation scheme, we demonstrate how both of these effects could be used for truly ultrafast coherent control of the motion of the magnetization. Moreover, these two nonthermal effects can also be combined as demonstrated in Sec. V C to achieve single-pulse switching of the magnetization on a femtosecond time scale.

III. THERMAL AND NONTHERMAL EFFECTS OF LIGHT ON MAGNETIZATION

A. Thermally induced quenching of magnetic order in $FeBO_3$

Due to its absorption peak in the vicinity of the excitation wavelength, iron borate happened to be a convenient material to study the thermally induced changes of magnetization. Measurements of the latter allowed us to determine the typical phonon-magnon relaxation time.

Note that the optical pump pulse influences both the magnetic and the optical properties of the excited medium. Because the output of the detection scheme used depends on the intensity of the probe beam, knowledge of the transient transmission is necessary. It was measured by using a single-diode response with amplitude modulation of the pump beam.

We then calibrated the measured time dependences of the Faraday rotation by dividing them by the associated transient transmissions (shown in Fig. 5a). The resulting data show a peak during the overlap of the pulses that is followed by a slow breakdown of the antiferromagnetic order.[1)] The amplitude of the initial peak was found to be a linear function of the pump fluence, as shown in Fig. 5b. The slow component of the Faraday rotation as a function of temperature and time is shown in Fig. 6. The dynamical changes of the Faraday effect are smaller at lower temperatures, while at $T=346.5$ K the Faraday rotation rapidly decreases until a delay of about 500 ps, where the signal vanishes.

The intrinsic Faraday effect is shown in Fig. 7 as a function of temperature. Since the Faraday rotation is proportional to the order parameter, its temperature dependence is generally given by[70]

$$\alpha_F(T) = \alpha_0\left(1-\frac{T_s}{T_N}\right)^{\beta}, \tag{7}$$

where T_N is the Néel temperature, β is the critical exponent, and T_s is the magnon temperature, which drives the order parameter. Fitting Eq. (7) to the corresponding measurements that are represented by solid squares in Fig. 7, we obtained $\beta=0.364\pm0.008$ and $T_N=347.0\pm0.1$ K. These values are in good agreement with $\beta=0.354$ and $T_N=348.35$ K reported before.[57]

Repeating those measurements at a negative delay of −20 ps, we obtained identical results but shifted about 10 K towards lower temperature. This offset was due to heat accumulation caused by the repeated excitation of the sample.

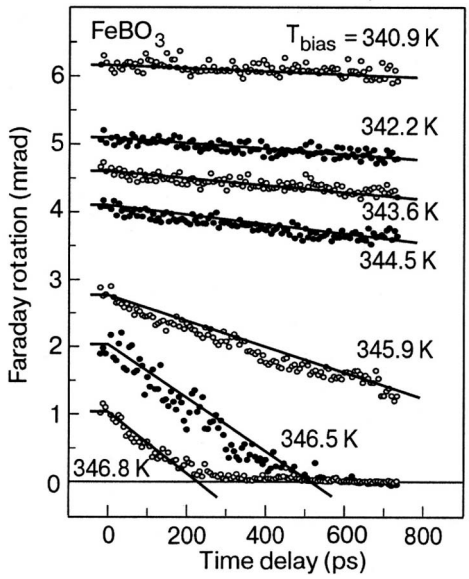

FIG. 6. The long-term transient Faraday rotation measured as a function of temperature. The antiferromagnetic order is destroyed at a time delay of 500 ps for $T=346.5$ K.[44]

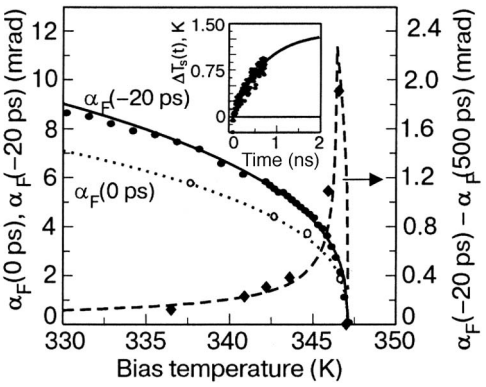

FIG. 7. The Faraday rotation without pump (solid squares) and at negative (solid circles) and zero (open circles) time delay as a function of the bias temperature with the fit to Eq. (7) (solid and dotted lines, respectively). The difference between the intrinsic magnetooptical signal and that at 500 ps is shown by diamonds together with the calculation based on the fitted parameters (dashed line). The inset shows the transient component of the magnon temperature as a function of the time delay. The solid line is the fit according to Eq. (8).[44]

We minimized this effect by using the lowest possible repetition rate that yielded a reasonable signal-to-noise ratio. The measured magnitude of the temperature offset was in good agreement with an estimate based on the optical and thermal properties of $FeBO_3$ and was added to T when plotting the relevant data.

Figure 7 also shows the difference between the intrinsic magnetooptical signal and that at a time-delay of 500 ps. This difference increases drastically before dropping to zero at the Néel point. All these features strongly imply that the pump-induced relaxation of the magnetooptical signal is related to an increase of the magnon temperature. At a temperature of $T=346.5$ K and at a delay time of 500 ps the Néel point is reached and antiferromagnetism is destroyed.

The temperature dependence of the Faraday rotation at zero time delay is shown in Fig. 7 by open circles. The experimental data were fitted by Eq. (7) with β and T_N deduced from the previous fit and the result of the fit is shown by the dotted line. The similarity of the temperature behavior of the intrinsic Faraday rotation and that at zero time delay strongly suggests that no magnetic excitation occurs within 100 fs.

This result proves that the time-resolved data (cf. Fig. 6) are not directly affected by the optical excitation itself, since the lifetime of the electrons in the excited state is shorter than 100 fs, as deduced from the huge linewidth of the ${}^6\Gamma_1^+ \rightarrow {}^4\Gamma_4^+$ transition. This estimate is justified by the dramatic changes of the absorption spectrum with temperature in Fig. 3, the fact that the transition takes place between states with different electronic configurations $(t_{2g})(e_g)^2 \rightarrow (t_{2g})^4(e_g)^1$, and earlier reports,[71] which all show that this transition is accompanied by the excitation of optical phonons and that it is intrinsically broad. Possible minor contributions due to inhomogeneous broadening are negligible.[71]

In order to derive information about the magnetization dynamics from the measured transient Faraday rotation $\alpha_F(t)$ plotted in Fig. 6, we converted the latter into transient magnon temperatures $T_s(t)$ by means of Eq. (7) for all data below T_N. Decomposing these temperatures into a static temperature T and an optically induced transient component $\Delta T_s(t)$, we found all $\Delta T_s(t)$ to be identical within the experimental error. Their average is shown in the inset of Fig. 7 and is characterized by a monotonic increase that was fitted by the function

$$\Delta T_s(t) = T_s^0\left(1 - \exp\left(-\frac{t}{\tau_{sl}}\right)\right), \tag{8}$$

where T_s^0 is the amplitude of the dynamical temperature and τ_{sl} is the phonon-magnon interaction time. All the variables were treated as fitting parameters, and the result of the fit for $T_s^0=1.4$ K and $\tau_{sl}=700$ ps is shown in the inset by a solid line.

Using the deduced parameters T_s^0, τ_{sl}, and α_0 we calculated the difference between the intrinsic Faraday rotation and that at a time delay of 500 ps as a function of temperature (dashed line in Fig. 7). Excellent agreement with the experimental data is found.

Due to ${}^6\Gamma_1^+ \rightarrow {}^4\Gamma_4^+$ excitation the electron potential energy increases only by 1.4 eV, while the excess of the photon energy is either transferred to the lattice or the magnetic system. Generally magnon-assisted transitions are less intense than phonon-assisted ones.[72] Consequently, after the optical excitation the temperature of the phonons is higher than that of the magnons: $T_l > T_s$. This difference gradually vanishes, and the magnon temperature increases with a time constant determined by the phonon-magnon interaction that is predominantly related to the relativistic spin-orbit coupling in a magnetic ions and affected by magnetostriction only in a limited spectral range near the center of the Brillouin zone.[73,74] We found that the phonon-magnon interaction in $FeBO_3$ has a characteristic time $\tau_{sl}=700$ ps.

A study of magnetization reversal by pulses of microwave radiation showed that the $FeBO_3$ lattice is thermally isolated from the magnetic subsystem during about 16 ns after excitation.[75] This value is a factor of 20 larger than the phonon-magnon interaction time obtained in the present work. This large difference originates from the fact that in our experiment the energy exchange between the magnons and phonons over the whole Brillouin zone is important, whereas in microwave experiments only magnons with small or zero wave vector are involved. As the collision integral for these quasiparticles is relatively small, due to the conservation of energy and momentum, the equilibration of spin and lattice temperatures can be 100 times faster than the decay of magnons with zero wave vector.[74]

Thus the photoexcitation of iron borate results in heating of the lattice via phonon-assisted transitions to the excited state and nonradiative relaxation. The antiferromagnetic order is subsequently destroyed via an energy transfer from the lattice to the magnetic subsystem that leads to an increase of the magnon temperature. This allows one to determine the phonon-magnon interaction time to be around 700 ps. This value is a factor of 20 smaller than found in experiments in the microwave region. The dynamics of the Faraday effect in the subpicosecond time domain is due to transitions of the Fe^{3+} ions to the excited low-spin state ($S=3/2$), which does not lead to any magnetic excitations because of fast relaxation of the ions to the ground state ($S=5/2$) within 100 fs.

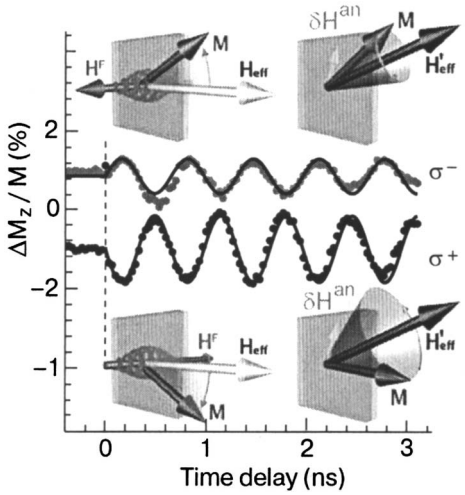

FIG. 8. Precession following excitation with circularly polarized light. The two helicities σ^+ and σ^- give rise to precessions with opposite phase and different amplitude. During the 100 fs presence of the laser pulse the magnetization precesses in the dominating axial magnetic field $\mathbf{H}^F$ created by the circularly pump pulse. Subsequent precession takes place in the effective magnetic field $\mathbf{H}'_{\text{eff}}=\mathbf{H}_{\text{eff}}+\delta\mathbf{H}^{\text{an}}$ (Refs. 50 and 51).

B. Nonthermal optical control of magnetization in magnetic garnets

1. Experimental observations

In contrast to iron borate, garnets show a minimum of absorption at the excitation wavelength. The key factor, however, in distinguishing the nonthermal effects described below was in their dependence on the pump pulse polarization. Thus, left- and right-handed circularly polarized laser pulses were used to excite the magnetic garnet film exposed to an in-plane applied magnetic field $\mathbf{H}_{\text{ext}}$. Precessions of $\mathbf{M}$ with opposite phases were triggered by pulses of helicity σ^- and σ^+; see Fig. 8. The initial phase of the signal reveals that $\mathbf{M}$ initially moves along the $\pm z$ direction, and therefore both $\mathbf{M}$ and $\mathbf{H}_{\text{eff}}$ are parallel to the film plane immediately after the photoexcitation.

Our experimental observations can be understood if during the presence of the laser pulse a strong magnetic field along the $\mathbf{k}$ vector of light is created. Such an axial magnetic field $\mathbf{H}^F$ can be generated by intense circularly polarized light through what is known as the inverse Faraday effect[10,76–78] (see below). In our experiment these optically generated field pulses are much stronger than both the anisotropy $\mathbf{H}_{\text{an}}$ and the applied field $\mathbf{H}_{\text{ext}}$ and therefore completely dominate during the $\Delta t=100$ fs presence of the laser pulse. The magnetization will respond by precessing in the plane of the film (normal to H_F) to a new in-plane orientation. After the pulse is gone, the magnetization will precess in the effective in-plane field $\mathbf{H}'_{\text{eff}}=\mathbf{H}_{\text{ext}}+\mathbf{H}_{\text{an}}+\delta\mathbf{H}^{\text{an}}$, as illustrated in Fig. 8.

The strength of the photoinduced field $\mathbf{H}^F$ can be estimated from the precession amplitude Λ:

$$H^F \approx \frac{\omega}{\gamma} \approx \frac{\Lambda}{\gamma \Delta t_{\text{pulse}}}, \tag{9}$$

where ω is the precession frequency, γ is the gyromagnetic ratio, and Δt_{pulse} is the duration of the optical pulse. We find that laser pulses of energy 20 μJ create transient magnetic field pulses of about 0.6 T in the garnet films.

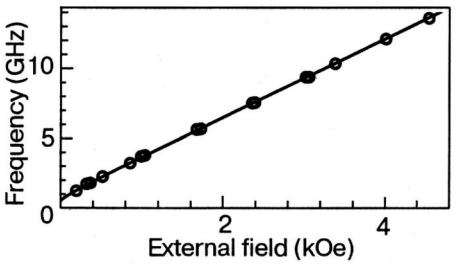

FIG. 9. Precession frequency as function of the externally applied magnetic field, measured with σ^+ polarized excitation. Circles represent measurements and the solid line is a best fit using $4\pi M_s=550$ G and $\mathbf{H}_{\text{an}}=50$ Oe.[51]

The consistently large-amplitude precession triggered by σ^+ polarized pump pulses, irrespective of the applied field strength $\mathbf{H}_{\text{ext}}$, allows the external field dependence of the precession frequency $\omega(H_{\text{ext}})$ to be accurately determined from the experimental data. As will be discussed in Sec. V C below, this is not the case for σ^- polarized excitation, which under certain conditions does not trigger any precession (see Fig. 27). The precession frequency is given by the Kittel formula[79] and can, for our geometry, be expressed as

$$\omega = \gamma\sqrt{BH} = \gamma\sqrt{(4\pi M_s + H'_{\text{an}} + H_{\text{ext}})(H'_{\text{an}} + H_{\text{ext}})}, \tag{10}$$

where the small photoinduced modification $\delta\mathbf{H}^{\text{an}}$ of the anisotropy field has been included in $H'_{\text{an}}=H_{\text{an}}+\delta H^{\text{an}}$. Figure 9 shows the measured ω as a function of the applied magnetic field for the σ^+ polarized pump excitation. The solid line represents a best fit using Eq. (10) and gives an $\mathbf{H}_{\text{an}}$ of about 50 Oe, in accordance with the results of Fig. 1.

2. Phenomenological model of the inverse Faraday effect

The normal Faraday effect can be viewed as due to a difference in the refractive indices for the two circularly polarized eigenmodes of light propagating in a magnetized medium. The inverse process, where circularly polarized light creates a magnetization or an effective magnetic field is also possible[10,77,78] and is known as the inverse Faraday effect. Strictly speaking, this effect is classified as an optomagnetic effect as it, in contrast to photomagnetic effects, does not depend on absorption.[49] Phenomenologically the creation of an axial magnetic field by circularly polarized light can be described as

$$\delta H_i^F(0) = \chi_{ijk}[E_j(\omega)E_k^*(\omega) - E_k(\omega)E_j^*(\omega)], \tag{11}$$

where χ_{ijk} is a third-rank axial tensor with nonzero components for crystals of any symmetry.[80] The magnetic field is created by elliptically or circularly polarized light along its $\mathbf{k}$ vector. The field changes sign when the circular polarization is changed from left-handed to right-handed. The effect does not rely on absorption but becomes possible due to strong spin-orbit coupling in a material. The optically induced magnetic field pulse appears to act only during the presence of the laser pulse in the material.[10] Its strength depends on the value of the relevant χ_{ijk} components and is directly related to the Verdet constant. For our garnet films we can estimate the optically induced effective field strength from the resulting precession dynamics. At the wavelength of 805 nm used

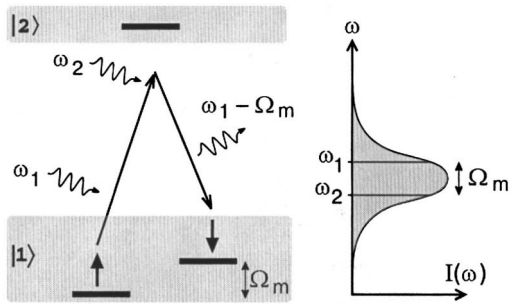

FIG. 10. Illustration of the stimulated Raman-like coherent scattering mechanism believed to be responsible for the ultrafast optically generated magnetic field. Two frequency components of electromagnetic radiation from the spectrally broad laser pulse take part in the process. The frequency ω_1 causes a transition to a virtual state with strong spin-orbit coupling. Radiation at the frequency ω_2 stimulates relaxation back to the ground state with the creation of a magnon.

in our experiments we find $H^F \approx 0.6$ T for a pump irradiance of about 10^{11} W/cm^2.

3. Microscopic model of the inverse Faraday effect

In this section we discuss a possible microscopic mechanism for the creation of an axial magnetic field by light and argue that it can be both efficient and ultrafast.

In the electric dipole approximation an optical transition cannot change the spin state of an electron. After electric dipole transitions the next most likely type of transition is a magnetic dipole transition, which is due to the interaction between the electron spin and the oscillating magnetic field of the incident electromagnetic radiation. Magnetic dipole transitions allow spin flip but typically are about 10^5 times less probable than similar electric dipole transitions. The strong effect that we see indicates a mechanism that allows change of the electron spin with higher efficiency than expected from a magnetic dipole transition. Moreover, the mechanism should not rely on material properties specific to garnets, as the reported effect has also been shown to exist in other magnetic materials such as rare earth orthoferrites[10] and metallic alloys.[36]

A stimulated Raman-like coherent optical scattering process has been suggested to account for both the speed and the efficiency of the excitation.[10,77,81,82] Two frequency components of electromagnetic radiation, both present in the 100 fs wide laser pulse, take part in the process (see Fig. 10). The frequency ω_1 stimulates an optical transition from the ground state $|1\rangle$ to a virtual state with a strong spin-orbit interaction. Due to this strong spin-orbit coupling there is a large probability of flipping the electron spin. Radiation at the frequency ω_2, also present in the optical pulse, stimulates relaxation back to the spin-split ground state with the electron spin reversed. The relaxation is accompanied by the coherent emission of a photon of energy $\hbar(\omega_1 - \Omega_m)$ and the creation of a magnon of energy Ω_m. This process can be much more efficient than a simple magnetic dipole transition, as it is coherently stimulated by radiation at the frequency ω_2 present in the laser pulse. Moreover, as the energy of the virtual state is of the order of the photon energy $E = \hbar\omega = 1.54$ eV, the transition can be fast, of the order of $\tau \sim h/E \sim 3$ fs.

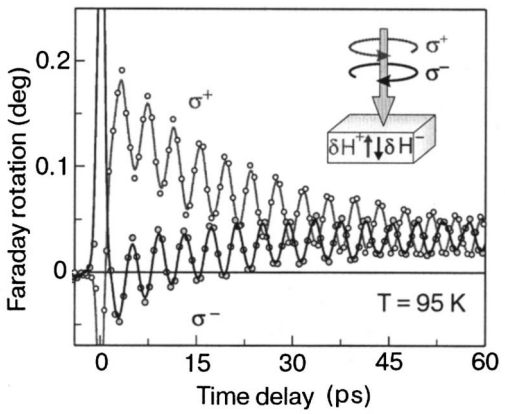

FIG. 11. Magnetic excitations in $DyFeO_3$ probed by the magnetooptical Faraday effect. Two processes can be distinguished: 1) instantaneous changes of the Faraday effect due to the photoexcitation of Fe ions and relaxation back to the high-spin ground state $S=5/2$; 2) oscillations of the Fe spins around their equilibrium direction with an approximately 5 ps period. The circularly polarized pumps of opposite helicities excite oscillations of opposite phase. The inset shows the geometry of the experiment. Vectors $\delta\mathbf{H}^+$ and $\delta\mathbf{H}^-$ represent the effective magnetic fields induced by right- and left-circularly polarized pumps, σ^+ and σ^-, respectively.[10]

C. Optical excitation of antiferromagnetic resonance in $DyFeO_3$

Thanks to this optomagnetic inverse Faraday effect, circularly polarized pulses can be used to excite magnetization dynamics in a situation when any other method is difficult or impossible to apply. Thus in this Section we describe optical excitation of different modes of antiferromagnetic resonance in $DyFeO_3$.

For the detection of the optically induced magnetization we used the direct magnetooptical Faraday effect, which was possible due to the presence of a weak ferromagnetic moment. Figure 11 shows the temporal evolution of the Faraday rotation in a z-cut $DyFeO_3$ sample for two circularly polarized pump pulses of opposite helicities. On the scale of 60 ps one can clearly distinguish two different processes that start after excitation with a pump pulse. At zero time delay, instantaneous changes of the Faraday rotation are observed which result from the excitation of virtual and real transitions in the Fe^{3+} ions from the high-spin ground state $S=5/2$. The instantaneous changes of the Faraday rotation are followed by oscillations with a frequency of about 200 GHz which can clearly be assigned to oscillations of the magnetization. It is seen from Fig. 11 that the helicity of the pump light controls the sign of the photo-induced magnetization. This observation unambiguously indicates that the coupling between spins and photons in $DyFeO_3$ is direct, because the phase of the spin oscillations is given by the sign of the angular momentum of the exciting photon.

Figure 12 shows the difference between the Faraday rotations induced by right- and left-circularly polarized pump light in the z-cut sample for the temperature range between 20 and 175 K. It is seen that an increase of the temperature results in an increase of the oscillation frequency to 450 GHz at 175 K, while the amplitude of the oscillations decreases. This behavior is in excellent agreement with previous Raman experiments[67,83,84] in $DyFeO_3$. The damping of the oscillations in the range of 200 ps is due to magnon scattering on

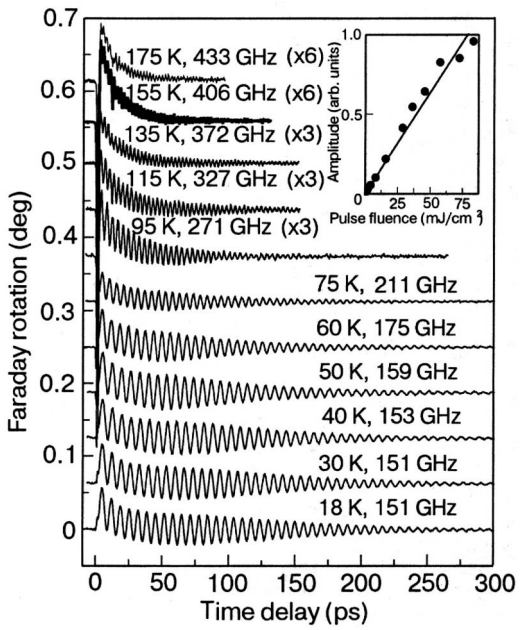

FIG. 12. Excitation of the spin oscillations in $DyFeO_3$ measured at different temperatures in the range between 18 and 175 K. In order to exclude effects not relevant to magnetic excitations, the difference between the signals for right- and left-circularly polarized pump pulses is plotted. Each new curve is shifted from the previous one along the vertical axis by 0.06°. The inset shows the amplitude of the spin oscillations as a function of pump fluence.[10]

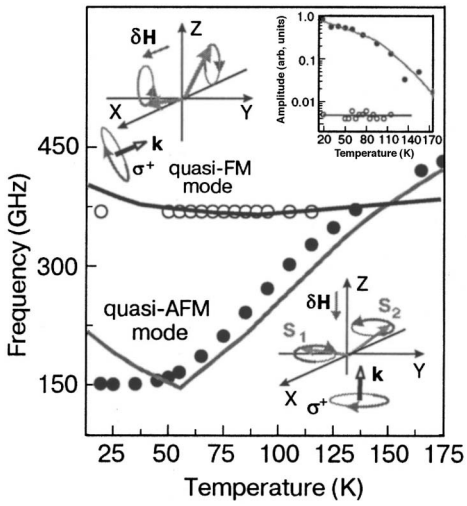

FIG. 13. Temperature dependence of the frequencies of the observed spin oscillations. Filled and open circles show the frequencies of the excited oscillations for laser pulses propagating along the z and x axis, respectively. Lines show the frequency of the quasi-antiferromagnetic (quasi-AFM) and the quasi-ferromagnetic (quasi-FM) resonance modes from Refs. 67, 83, and 84. Top right inset shows the temperature dependence of the oscillation amplitudes. Top left and bottom right insets are, respectively, schematic representations of the quasi-FM and quasi-AFM modes of the spin resonance. Vectors $\delta\mathbf{H}$ show the directions of the instantaneous magnetic field that is equivalent to the photoexcitation.[10]

phonons and on the spins of dysprosium ions. The highest value of the amplitude of the photoinduced oscillations is observed between 20 and 50 K. The amplitude of the oscillations corresponds to a photoinduced change of the magnetization $\Delta M \sim 0.06 M_s$, where M_s is the saturation magnetization. This ratio is obtained from hysteresis measurements in a static magnetic field, which show that the saturated Faraday rotation in a single-domain z-cut sample is about $\sim 1°$.

From Figs. 11 and 12 one can distinguish not only oscillations but also an exponential decay of the equilibrium level on a time scale of about 100 ps. This can be explained by a photoinduced change of the equilibrium orientation of the magnetization and subsequent decay of the equilibrium orientation to the initial state. Although in principle the effect of optically induced magnetization does not require the absorption of photons, the laser control of the spontaneous magnetization and the excitation of coherent spin oscillations are equivalent to photoexcitation of magnons and thus require some energy. The inset in Fig. 12 shows the amplitude of the photoexcited spin oscillations as a function of the pump intensity. The linearity of this dependence indicates that the photoexcitation of magnons is a one-photon process. Note that extrapolation of the intensity dependence shows that the photoinduced effect on the magnetization would reach the saturation value of M_s at a pump fluence of about 500 mJ/cm^2. The effect of such 100 fs laser pulse on the magnetic system would be equivalent to the application of a magnetic field pulse of about 5 T. According to our measurements, the absorption in $DyFeO_3$ in the near infrared spectral range is on the order of 100–200 cm^{-1}. Given this low value of the absorption, a photoexcitation of 500 mJ/cm^2 is still below the damage threshold of $DyFeO_3$ and thus quite feasible, provided a sample of high optical quality is available.

Due to the strong anisotropy of the magnetic susceptibility in $DyFeO_3$, magnetic field pulses in different directions should trigger different types of spin oscillations (Fig. 13). A magnetic field pulse directed along the z axis excites oscillations that correspond to the quasi-antiferromagnetic resonance mode, while a field pulse along the x axis will excite the quasi-ferromagnetic resonance mode.[67] These predictions are in excellent agreement with the experimentally observed temperature dependences of the oscillation frequency for z-cut and x-cut samples. These closely resemble the temperature dependence for the quasi-antiferromagnetic and the upper quasi-ferromagnetic resonance mode in $DyFeO_3$, respectively (see Fig. 13).

Note that the application of a static external magnetic field up to 0.5 T in a direction parallel to the wave vector of light resulted in only a slight change of the frequency (about 1%), again confirming that the effective photoinduced field is dominating the dynamics.

It is thus clear that with circularly polarized femtosecond laser pulses one can purely optically and thus nonthermally excite and coherently control the antiferromagnetic precession. Using circularly polarized photons one can affect an ensemble of strongly correlated spins, excite coherent spin oscillations, and control the phase of these oscillations with the helicity of light. The decisive proof of this direct coupling is that the phase of the spin oscillations is controlled by the sign of the angular momentum of the exciting photons and changes sign on going from right to left helicity of the exciting laser pulse. This mechanism was discussed above in Sec. III B. Such optical pulses are shown to be equivalent to magnetic field pulses of large amplitude. In view of the great variety of magnetic materials, the direct effect of light on the spontaneous magnetization in other materials and at higher temperatures is foreseen. Our findings open new insights into

the understanding of ultrafast magnetic excitation and, in view of recent progress in the development of compact ultrafast lasers,[11] may provide new prospects for applications of ultrafast photomagnetic phenomena.

IV. LASER-INDUCED CHANGES OF MAGNETIC ANISOTROPY

In contrast to the previous Section, where the laser pulse was affecting the magnetization itself, whether thermally or nonthermally, here we deal with the laser-induced changes of the magnetic anisotropy. That is, the laser pulse changes the equilibrium direction of the magnetization, thus forcing the latter to precess around this new equilibrium.

A. Thermally induced spin reorientation in $TmFeO_3$

The temperature-dependent anisotropy energy in $TmFeO_3$ has the form[85,86]

$$F(T) = F_0 + K_2(T)\sin^2\theta + K_4\sin^4\theta, \tag{12}$$

where θ is the angle in the xz plane between the x axis and the AFM moment $\mathbf{G}$ (see Fig. 2), and K_2 and K_4 are the anisotropy constants of second and fourth order, respectively. Applying equilibrium conditions to Eq. (12) yields three temperature regions corresponding to different spin orientations:

$$\Gamma_4(G_xF_z):\ \theta = 0, \quad T \geqslant T_2,$$

$$\Gamma_2(G_zF_x):\ \theta = \frac{1}{2}\pi, \quad T \leqslant T_1,$$

$$\Gamma_{24}:\ \sin^2\theta = -\frac{K_2(T)}{2K_4}, \quad T_1 \leqslant T \leqslant T_2, \tag{13}$$

where T_1 and T_2 are determined by the conditions $K_2(T_1) = -2K_4$ and $K_2(T_2) = 0$ and the Γ's indicate the representations of the respective symmetry groups.[87] Therefore, depending on the anisotropy constants, a spin reorientation that shows two second-order phase transitions, at T_1 and T_2, may be expected. The temperature dependence of θ in the phase Γ_{24} is determined by $K_2(T)$, which varies roughly linearly with temperature.[62]

As also shown in Fig. 2, the transition between the two spin configurations in the antiferromagnet can be monitored with the help of linear birefringence, when the refractive index n of a medium depends on the orientation of the light polarization. For light propagating along the z axis through a birefringent medium, the refractive indices for light polarized along the x axis and the y axis are different; here Δn_{xy} characterizes the birefringence and is determined by the difference of the diagonal components of the dielectric permittivity tensor:

$$\Delta n_{xy} = \frac{\varepsilon_{xx} - \varepsilon_{yy}}{2n}. \tag{14}$$

Regarding the change of the diagonal components induced by the presence of the AFM vector $\mathbf{G}$, that is $\varepsilon_{ii} = \varepsilon_{ii}^{(0)} + \beta_{iijk}G_jG_k$, one can find for $TmFeO_3$ that $\Delta n(\Gamma_2) \neq \Delta n(\Gamma_4)$. Thus the birefringence serves as a direct measure of the orientation of the AFM vector $\mathbf{G}$.

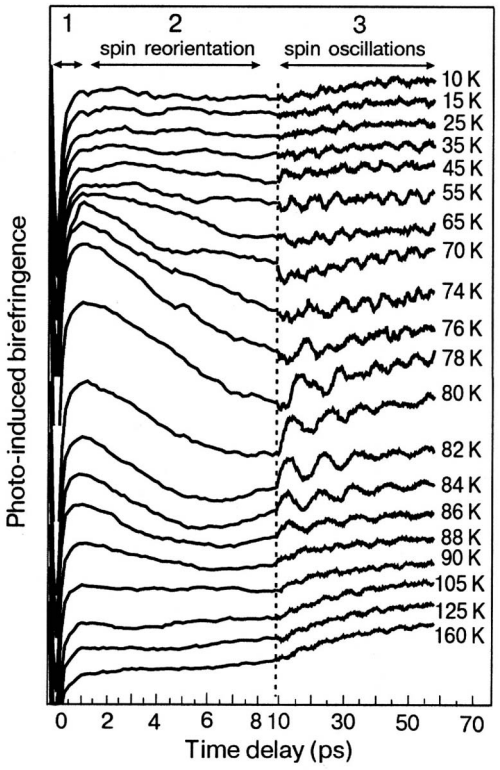

FIG. 14. Excitation and relaxation of the AFM moment measured via changes in the magnetic birefringence. On the figure one can distinguish three processes: 1) electron-phonon thermalization with 0.3 ps relaxation time; 2) rotation of the AFM vector with 5 ps response time; 3) oscillations of the AFM vector around its equilibrium direction with an approximate 10 ps period.[9]

Measurements of the absorption showed that at a photon energy of 1.55 eV, the laser pulse is absorbed in the sample via the excitation of the localized electronic states of the Fe^{3+} and Tm^{3+} ions. The resulting changes of the birefringence are summarized in Fig. 14.[9] In the time domain, the relaxation process can be divided in three distinct regions. First, the excitation decays via phonon cascades, and the phonon system thermalizes in a very short time (process 1 in Fig. 14, with a time constant of around 0.3 ps). This time is in approximate agreement with earlier results.[44] The phonon-phonon interaction sets a new lattice temperature, and so the equilibrium anisotropy axis is changed. Under such conditions in a FM material, the magnetization vector would precess around its new equilibrium direction, approaching it as a result of the damping (see Fig. 15).[88] In an antiferromagnet, the exchange-coupled spins start to precess in opposite directions, thus creating a strong exchange torque $\mathbf{T}_{ex}$ that opposes this precession (see Fig. 15). The resulting motion of the spins to the new equilibrium should then occur in the plane spanned by $\mathbf{H}_A$ and $\mathbf{S}$. This process is marked 2 in the time dependences in Fig. 14 and has a characteristic time of about 4 ps. This relaxation time corresponds to an AFM resonance frequency of 80 GHz. The amplitude of this spin reorientation reaches 30 degrees in our experiment (see Fig. 16), this value being obtained with the help of the static birefringence data from Fig. 2.

After the initial relaxation, the antiferromagnetic vector oscillates around its new equilibrium (process 3), with

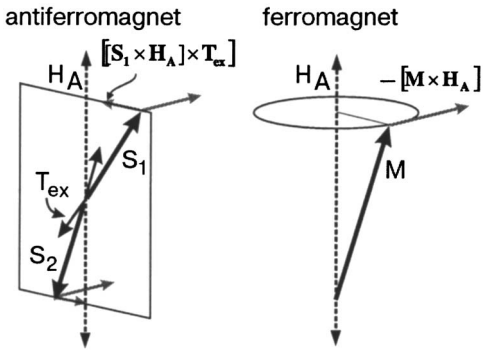

FIG. 15. Schematic illustration of the spin relaxation in an antiferromagnet as compared to that in a ferromagnet: in contrast to the spiral FM precession, the AFM vector moves in a plane.[9]

temperature-dependent frequency and amplitude. Particularly strong oscillations are observable in the range 80–90 K, i.e., in the region of the reorientational transition (Fig. 16). In fact, the temperature dependence of the derived frequencies should closely resemble that of spin waves with $k=0$, shown by a thin line in Fig. 16.[86] Such spin waves are equivalent to the homogeneous magnetization precession observed under such conditions in ferromagnets.[29] In our case, however, the amplitudes of the oscillations are so large, up to ten degrees, that the observed modes are quite different from small-amplitude spin waves. As a matter of fact, the damping of such large-amplitude AFM oscillations is expected to differ from that of the AFM resonance and should be studied separately.

Note that Fig. 11 also shows that the frequencies of the oscillations may increase with delay time, as is particularly visible for the data at $T=78$ K. This can easily be understood, because the optically induced temperature increase pushes the AFM vector into the reorientation region. Therefore, the starting frequency is low. During the process of relaxation, however, the temperature decreases and restores the effective anisotropy field value, resulting in the observed frequency increase.

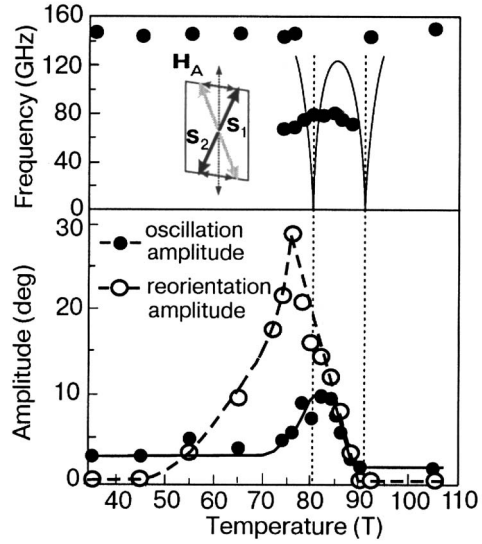

FIG. 16. Temperature dependences of the amplitudes and frequencies of the observed oscillations, as well as the amplitude of the spin reorientation. Thin line shows the frequency change at the reorientational transition from Ref. 86. Inset shows the oscillations of spins in the xz plane. Nonzero reorientation amplitude at $T=55$ K corresponds to an instantaneous local laser-induced heating of more than 25 K.[9]

The experiment shows that the AFM spins in $TmFeO_3$ are reoriented by several tens of degrees during only a few picoseconds. For comparison, in a ferromagnet with an anisotropy energy similar to that of $TmFeO_3$ (10^4 J/m^3)[57] the magnetization precesses with a period of several hundred picoseconds.[6,89]

We should also remember here that a relaxation time of about 700 ps was measured for the laser-induced destruction of the AFM order in $FeBO_3$ (see Sec. III A above). In contrast, the spin reorientation happens to be a much faster process.

The measured maximum of the reorientation amplitude of 30 degrees, in fact, is only related to the problem of the instantaneous and homogeneous heating of a bulk sample and can easily be overcome in smaller structures, where such reorientation is of practical importance. For example, in an exchange-coupled FM/AFM bilayer, the laser-induced reorientation of the AFM vector by 90 degrees will trigger, via the exchange coupling, a precession of the FM moment into the opposite state.[9] Thus, in addition to increasing the stability of magnetic nanoelements,[90] the AFM layer can also play an active role in the switching process.

Thus an ultrafast spin reorientation in antiferromagnetic $TmFeO_3$ can be induced by a laser pulse. Optical excitation leads, via electron-phonon relaxation and phonon-phonon interaction processes, to a subpicosecond change of the anisotropy axis. Such change is equivalent to an ultrafast magnetic impact. It has also been shown that the linear magnetic birefringence appears to be a sensitive experimental technique to study the motion of the AFM vector. Thus the dynamics of the AFM moment can be influenced and detected by an all-optical pump-probe method. Last, but not least, in contrast to the spins in a ferromagnet, the AFM spins can be fully reoriented within a few picoseconds, without the application of an external magnetic field.

B. Ultrafast modification of anisotropy via direct photomagnetic interaction

The dynamics of $TmFeO_3$ just described was caused by a laser pulse that could be of any polarization, via a heat-induced phase transition. It is a dependence on the pump pulse polarization, however, which is the fingerprint of a nonthermal effect. Such nonthermal modification is clearly demonstrated in thin garnet films, with a laser wavelength in the transparency region.

1. Experimental observations

By applying an external magnetic field $\mathbf{H}_{ext}$ in the plane of a magnetic garnet sample (so that $\mathbf{M}$ is in-plane, $\zeta=90°$) and pumping with linearly polarized laser pulses, optically triggered precession of the magnetization $\mathbf{M}$ was observed (see Fig. 17a). In the optical transmittivity of the sample (see Fig. 17c) a sudden drop is seen which does not relax significantly within 3 ns. Intriguingly, the amplitude and phase of the precession in Fig. 17a was found to depend on the plane of polarization θ of the pump pulses, as shown in Fig. 17b. Negative values of the amplitude indicate precession of $\mathbf{M}$

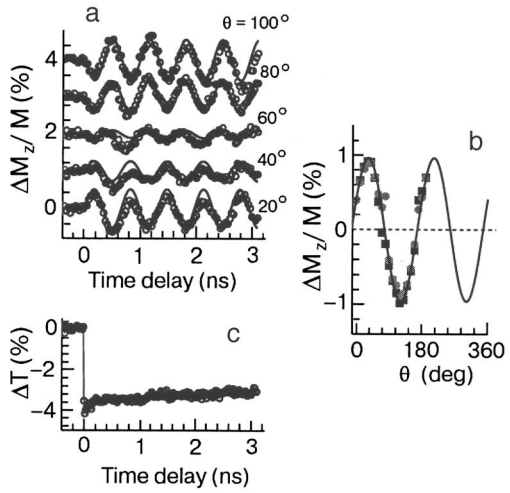

FIG. 17. Coherent precession of the magnetization triggered by linearly polarized laser pulses. (a) Time dependence of the precession for different planes of pump polarization θ, with an applied field of $|\mathbf{H}_{ext}|=350$ Oe in the plane of the sample. Circles represent measurements and solid lines simulations based on the Landau-Lifshitz equation. (b) Precessional amplitude as a function of the plane of polarization of the pump. Round and square symbols represent amplitudes extracted from measurements at $\pm\mathbf{H}_{ext}$. The solid line is a best fit. (c) Pump-induced change of the sample transmissivity ΔT.[51]

with the opposite phase. Maxima of the precessional amplitude (of opposite phase) were observed for every 90° rotation of the polarization, and at some polarizations no precessional dynamics was triggered. From this dependence on pump polarization it is evident that the underlying effect must be nonthermal. An ultrafast heating effect would only reduce the magnitude of the magnetization and the anisotropy field independently of the pump polarization. Heating effects thus cannot be responsible for triggering magnetization dynamics that exhibit polarization dependence of the type that we observe in Fig. 17.

It is also interesting to note that $\mathbf{M}$ always starts its precessional motion by moving normal to the film plane, along the $\pm\hat{z}$ direction. This follows from the initial phase of the measured signal in Fig. 17a, which always starts from the inflection point where M_z is changing most rapidly. From the Landau-Lifshitz equation [Eq. (2)] it can be inferred that immediately after the photoexcitation both $\mathbf{M}$ and $\mathbf{H}_{eff}$ are in the film plane but not parallel to each other. Consequently, the observed magnetization dynamics must be due to an ultrafast change of the magnetization $\delta\mathbf{M}$, the anisotropy field $\delta\mathbf{H}^{an}$, or a combination of the two, that effectively creates an in-plane angular displacement $\Lambda=\angle(\mathbf{M},\mathbf{H}_{eff})$ between $\mathbf{M}$ and $\mathbf{H}_{eff}$. It is possible to distinguish between these possibilities by analyzing the precession amplitude Λ as function of the applied field. The result is shown in Fig. 18. If triggered by an ultrafast rotation of the magnetization $\mathbf{M}\rightarrow\mathbf{M}+\delta\mathbf{M}$, the amplitude Λ of the subsequent precession should be independent of the strength of the applied magnetic field as $\angle(\mathbf{M},\mathbf{H}_{eff})$ does not depend on $\mathbf{H}_{ext}$. However, if the precession is caused by a change in the effective field through a photoinduced anisotropy field $\delta\mathbf{H}^{an}$, the precession amplitude Λ is expected to decrease with increasing applied magnetic field as

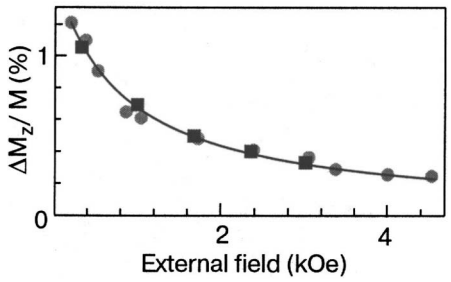

FIG. 18. Dependence of the precessional amplitude on the applied in-plane magnetic field $\mathbf{H}_{ext}$. Round and square symbols represent amplitudes extracted from measurements at $\pm\mathbf{H}_{ext}$.

$$\Lambda=\angle(\mathbf{H}_{eff},\mathbf{H}_{eff}+\delta\mathbf{H}^{an})\propto\frac{1}{|\mathbf{H}_{ext}+\mathbf{H}_{an}|}, \tag{15}$$

which is valid for small-amplitude precessions. As shown by the fitted curve in Fig. 18 (solid line) the measurements exhibit the exact behavior that one expects for a photoinduced anisotropy field $\delta\mathbf{H}^{an}$ [See Eq. (15)]. Based on the precession amplitude, the magnitude of the photoinduced field can be estimated as $\delta\mathbf{H}^{an}=0.5$ Oe for the present geometry ($\zeta=90°$). A graphical illustration of the excitation process and the subsequent precession is shown in Fig. 19.

For the present geometry, with the applied field in the plane of the film, changing the polarity of the magnetic field $\mathbf{H}_{ext}$ does not affect the measured signal for any given polarization of the pump. The fact that the precession phase and amplitude are both unaffected by reversing the polarity of the external field (see Fig. 17b) shows that $\delta\mathbf{H}^{an}$ must be odd with respect to $\mathbf{M}$: upon a change of the polarity of the external field, both $\mathbf{M}$ and the anisotropy field $\mathbf{H}_{an}$ in Eq. (3) change sign. It then follows from Eq. (2) that the photoinduced $\delta\mathbf{H}^{an}$ also must change sign, i.e., $\delta\mathbf{H}^{an}\rightarrow-\delta\mathbf{H}^{an}$ in order to give rise to the same signal.

By applying the external field at an angle with respect to the film plane, the magnetization can be tilted out of the film plane ($\zeta<90°$). The actual angle ζ that the magnetization makes with the film normal is determined by the balance between the applied field, the anisotropy field, and the demagnetizing field. When pumping with linearly polarized laser pulses in this configuration, a larger amplitude precession was observed (see Fig. 20a). This precession is superimposed on a slowly decaying exponential background caused by the relaxation of the photoinduced anisotropy. In contrast to the in-plane applied field geometry (where $\zeta=90°$), the initial phase of the precession in Fig. 20a reveals that for $\mathbf{M}$ tilted out of the film plane ($\zeta<90°$) the initial motion of $\mathbf{M}$ is nearly parallel to the film plane. This implies that the laser-induced $\delta\mathbf{H}^{an}$ is directed essentially along the z direction.

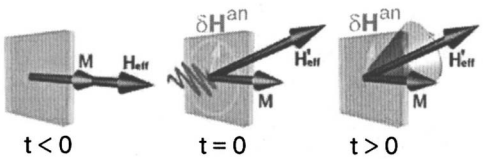

FIG. 19. Graphical illustration of the process of photoinduced magnetic anisotropy caused by linearly polarized laser excitation and the subsequent precessional dynamics.

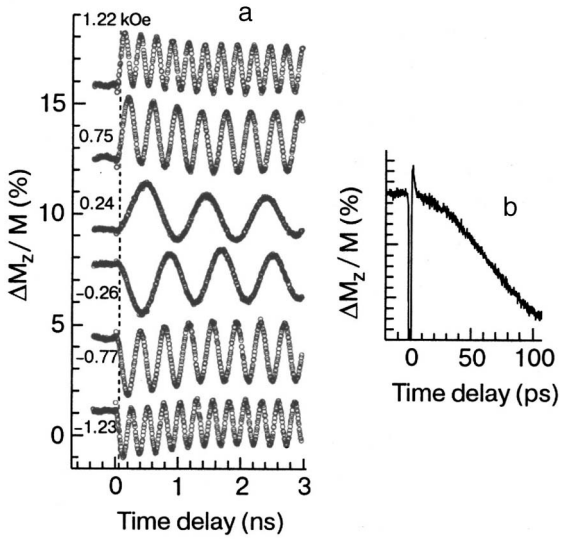

FIG. 20. (a) Precession of the magnetization following excitation with linearly polarized light for different values of the magnetic field applied at an angle of about 45° with the sample normal. (b) The excitation shown on a finer time scale.[51]

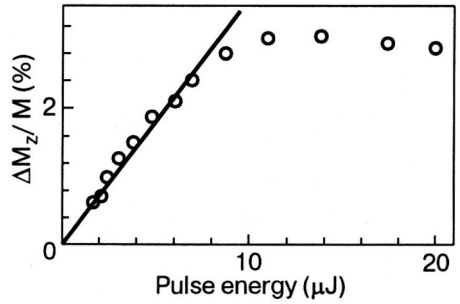

FIG. 21. Dependence of the precession amplitude on the excitation pulse energy.[51]

The dependence of the precession amplitude and phase on the polarization of the pump pulses becomes gradually smaller as **M** is tilted further out of the film plane. At about $\zeta=60°$, all polarization dependence is practically gone, and changing the polarity of the external field gives a near 180° phase shift in the measured signal. The diminishing influence of the pump polarization is caused by the dominating z component of $\delta\mathbf{H}^{an}$ and will be discussed further in Sec. IV B 2. From the precession amplitude in Fig. 20a, the strength of the photoinduced anisotropy field is estimated to be $\delta\mathbf{H}^{an}=1.5$ Oe.

Laser heating effects in the sample, if present, are likely to be more pronounced in this geometry than in the in-plane field geometry as a thermal reduction of **M** also changes the equilibrium $\mathbf{H}_{eff}$ and leads to a reorientation of **M** along the z direction. However, in our experiments the optical excitation of coherent spin waves is ultrafast (see Fig. 20b, where very fast initial relaxation of less than a few picoseconds is indicated), much faster than the phonon-magnon interaction time which is about 1 ns in this material,[45] and therefore cannot be of thermal origin. As was discussed above in Sec. III A (see also Ref. 51), thermal effects can be seen on the time scale of a nanosecond when the sample is heated to temperatures near the Curie point.

Based on the results in Fig. 20a one can argue that the lifetime τ of $\delta\mathbf{H}^{an}$ is longer than the time $t_{exp}=3$ ns accessible in this experiment. As the precession of **M** is always around the effective magnetic field $\mathbf{H}'_{eff}=\mathbf{H}_{eff}+\delta\mathbf{H}^{an}$, any relaxation of $\delta\mathbf{H}^{an}$ should be visible in the time trace of the precession. Note in Fig. 20a how **M** precesses around an equilibrium $\mathbf{H}'_{eff}$ that is different from the initial $t<0$ state. Some relaxation of $\mathbf{H}'_{eff}$ can be seen (the slow overall change of the fast oscillating signal) but is not sufficient to restore the original equilibrium on the time scale of the experiment. This indicates that after $t_{exp}=3$ ns $\delta\mathbf{H}^{an}$ has still not decayed completely. Another observation that supports this conclusion is the photoinduced change in the sample transmittivity ΔT shown in Fig. 17c, which also does not relax significantly during 3 ns.

There appears to be a linear relation between the precession amplitude and the pump power (Fig. 21) up to pulse energies of almost 10 μJ. At higher pulse energies the effect saturates completely. Based on the absorption coefficient the estimated density of absorbed photons is about one per hundred unit cells in the illuminated crystal volume. Saturation effects are therefore not expected unless they are caused by the presence of low-concentration impurities. This will be discussed in more detail in Sec. IV B 3 on the microscopic basis of the photomagnetic effect.

2. Phenomenological model of photoinduced magnetic anisotropy

In this subsection we give a macroscopic phenomenological description of the observed photoinduced magnetic anisotropy. The model is not concerned with the microscopic mechanism of the effect, but gives some insight into its symmetry properties.

The creation of a static magnetic field $\delta\mathbf{H}^{an}(0)$ in the sample can be described as a combination of the nonlinear process of optical rectification[91] and a linear magnetoelectric effect:[92]

$$\delta H_i^{an}(0)=\chi_{ijkl}E_j(\omega)E_k(\omega)M_l(0). \tag{16}$$

Here E is the electric field component of the light and M is the magnetization of the garnet film. The fourth-rank polar tensor χ_{ijkl} has nonzero components for crystals of any symmetry.[80]

When taking the experimental geometry (Fig. 4) and the symmetry of χ_{ijkl} for the $4mm$ point group of our samples into account, only four independent nonzero components of the tensor χ_{ijkl} remain,

$$A=\chi_{xxxx}=\chi_{yyyy},$$

$$B=\chi_{xyxy}=\chi_{xxyy}=\chi_{yxyx}=\chi_{yyxx},$$

$$C=\chi_{xyyx}=\chi_{yxxy},\quad D=\chi_{zxxz}=\chi_{zyyz}, \tag{17}$$

and the vector components of the photoinduced anisotropy field are then given by

$$\delta H_x^{an}\propto E_0^2M_s\sin\zeta[(A+C)\cos\varphi+(A-C)\cos 2\theta\cos\varphi + 2B\sin 2\theta\sin\varphi], \tag{18}$$

$$\delta H_y^{\text{an}} \propto E_0^2 M_s \sin\zeta[(A+C)\sin\varphi - (A-C)\cos 2\theta \sin\varphi + 2B \sin 2\theta \cos\varphi], \quad (19)$$

$$\delta H_z^{\text{an}} \propto E_0^2 M_s D \cos\zeta. \quad (20)$$

Here δH_i^{an} is the photoinduced field along the i direction, $\mathbf{i}=\{x,y,z\}$ refers to the crystal axes of the sample, φ denotes the azimuthal angle between the sample x axis and the projection of the magnetization vector on the film plane, and ζ is the angle between the film normal and the magnetization, as shown in Fig. 4.

From these equations one can see that if the magnetization $\mathbf{M}$ is in the film plane, the out-of-plane component δH_z of the photoinduced anisotropy field does not contribute, as $\cos\zeta=0$. This is in accordance with our experimental results from Fig. 17, which show an in-plane $\delta\mathbf{H}^{\text{an}}$. However, in order for the above equations to describe a field $\delta\mathbf{H}^{\text{an}}$ consistent with the polarization dependence of the precession amplitude, shown in Fig. 17b, the number of independent tensor components must be further reduced. The fact that there is no amplitude offset in the curve shown in Fig. 17b requires that $A=-C$, so that the first term in Eqs. (18) and (19) vanishes. Furthermore, the sinusoidal shape of the curve implies that $A=B$ and leaves us with only two independent components of the tensor χ_{ijkl}:

$$A = \chi_{xxxx} = \chi_{yyyy} = -\chi_{xyyx} = -\chi_{yxxy} = \chi_{xyxy} = \chi_{xxyy} = \chi_{yxyx} = \chi_{yyxx},$$

$$D = \chi_{zxxz} = \chi_{zyyz}. \quad (21)$$

These additional equalities indicate that the χ_{ijkl} tensor has a higher symmetry than the garnet crystal. However, this does not violate Neumann's principle, which states that the symmetry elements of any physical property of a crystal must include all the symmetry elements of the point group of the crystal. This does not prevent that property from having a higher symmetry than the crystal. The optically induced anisotropy field can now be written as

$$\delta H_x^{\text{an}} \propto A E_0^2 M_s \sin\zeta(\sin 2\theta \sin\varphi + \cos 2\theta \cos\varphi), \quad (22)$$

$$\delta H_y^{\text{an}} \propto A E_0^2 M_s \sin\zeta(\sin 2\theta \cos\varphi - \cos 2\theta \sin\varphi), \quad (23)$$

$$\delta H_z^{\text{an}} \propto D E_0^2 M_s \cos\zeta. \quad (24)$$

For the in-plane field geometry ($\cos\zeta=0$) this describes a vector of constant length and with a direction depending on the angle φ of the magnetization with respect to the x axis and the plane of polarization θ of the pump pulses. The δH_z^{an} component accounts for the observed behavior in Fig. 20 with the applied field at an angle so that $\zeta<90°$.

Computer simulations based on this simple model and the numerical integration of Eq. (2) exhibit good agreement with our experimental results, both for the in-plane $\mathbf{H}_{\text{ext}}$ geometry shown in Fig. 17a, where the results of the simulation are shown by solid lines, and for the out-of-plane $\mathbf{H}_{\text{ext}}$ geometry in Fig. 20 (simulations are not shown). The latter indicate that the tensor component D is larger than A by a factor of 3. This is not surprising in view of the symmetry distortion along the z axis known to exist in films of this type.[54,55,93]

One could have noted above, in Fig. 8, that circularly polarized pulses of opposite helicity excite precession of somewhat different amplitude. In order to understand this, we analyze our model of the photoinduced anisotropy [see Eq. (16)] for circularly polarized light $\mathbf{E}=E_0/(\hat{x}+i\hat{y})\sqrt{2}$:

$$\delta H_x^{\text{an}} \propto A E_0^2 M_s \sin\zeta \cos\varphi, \quad (25)$$

$$\delta H_y^{\text{an}} \propto -A E_0^2 M_s \sin\zeta \sin\varphi, \quad (26)$$

$$\delta H_z^{\text{an}} \propto D E_0^2 M_s \cos\zeta. \quad (27)$$

We find that a photoinduced $\delta\mathbf{H}^{\text{an}}$ that depends only on the direction φ of $\mathbf{M}$ with respect to the crystal axes can still exist. This is reasonable, as θ has no meaning for circularly polarized light. For an in-plane magnetization the photoinduced $\delta\mathbf{H}^{\text{an}}$ is parallel to the film plane. However, it does not depend on the helicity of the light and can therefore not account for the opposite phase of precession induced by light of opposite helicities.

The asymmetry seen in the signal amplitude between the σ^+ and σ^- helicities in Fig. 8 stems from the simultaneously created photoinduced anisotropy $\delta\mathbf{H}^{\text{an}}$ which is independent of the pump helicity [See Fig. 8 and Eqs. (25)–(27)]. For the σ^- helicity $\mathbf{M}$ precesses in the direction of the optically modified effective field $\mathbf{H}'_{\text{eff}}$ during the existence of $\mathbf{H}^F$. This gives rise to a precession with a small amplitude around $\mathbf{H}'_{\text{eff}}$ after the pulse is gone. For the σ^- helicity $\mathbf{M}$ precesses in the opposite direction during the existence of $\mathbf{H}^F$, moving further away from $\mathbf{H}'_{\text{eff}}$. After the pulse is gone, a large amplitude precession sets in.

3. Microscopic justification

Photomagnetic effects are known to exist in garnets containing certain dopants,[94,95] in particular Si and Co.[47,48] Optically induced electron transfer between ions on nonequivalent sites in the crystal is believed to cause a change in the magnetocrystalline anisotropy due to a redistribution of ions.[96] This effect is strong in crystals doped with elements that can assume different valence states, and where their contribution to the anisotropy is different. However, it has also been observed in undoped garnet samples containing Pb impurities,[97] which we believe is the case in our experiments.

The linear dependence of $\delta\mathbf{H}^{\text{an}}$ on the pump power shown in Fig. 21 suggests that linear optical absorption is the dominating absorption process. The saturation of $\delta\mathbf{H}^{\text{an}}$ at high pump intensities may be attributed to the Pb impurities. Divalent Pb^{2+} ions substitute trivalent Lu^{3+} ions on dodecahedral sites in the crystal and act as electron acceptors. This is a p-type doping which creates holes that are usually assumed to be located on iron ions in tetrahedral sites.[46,98] To maintain overall charge neutrality in the crystal, some tetrahedrally coordinated trivalent iron ions change their valency to 4+. Photoexcitation can induce a charge transfer between these Fe^{4+} ions and Fe^{3+} magnetic ions on octahedral sites, thus effectively "moving" the Fe^{4+} ions to sites with different symmetry (see Fig. 22), and thereby causing a change in the magnetic anisotropy.

The low concentration of Pb impurities creates a limited number of photoactive ions and the photomagnetic effect can

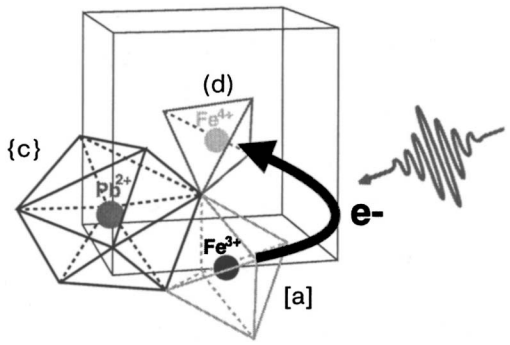

FIG. 22. Illustration of the photoexcitation of electrons between iron ions in different crystallographic sites. A laser pulse induces electron transfer from a Fe^{3+} ion in the octahedral site (denoted by [a]) to a Fe^{4+} ion in the tetrahedral site (denoted by (d)). The dodecahedral site with the divalent lead impurity is denoted by {c}.

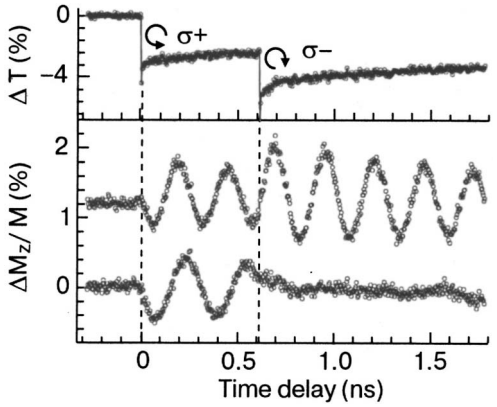

FIG. 23. Double pump experiment with circularly polarized laser pulses of opposite helicity and 15 μJ pulse power. The upper panel shows the pump-induced change of the sample transmissivity due to the photoexcitation of impurities. The lower panel shows how amplification and complete stopping of the magnetization precession can be achieved depending on the phase of the precession when the second laser pulse arrives. The time delay between the two pump pulses is fixed at approximately 0.6 ns, and the precession frequency is controlled by varying the external field.[51]

therefore be expected to saturate under intense illumination. An estimate for our sample shows that the illuminated volume of garnet film contains about 10^{12} Pb ions. An optical pulse of 20 μJ delivers 10^{14} photons, of which about 1% are expected to be absorbed. This allows, in principle, for all of the photoactive ions to be excited, and it is thus not surprising that saturation can occur at these pump intensities. The pump-induced change in transmissivity is also believed to be related to the photoexcitation of impurities.[99]

Finally, we would like to note that an ultrafast effect of light on magnetic anisotropy has been also observed in the antiferromagnetic dielectric NiO.[100]

V. COHERENT CONTROL OF MAGNETIC PRECESSION

The primary advantage of the nonthermal control of spins is the possibility of very high repetition rates, without the need to wait for the heat dissipation usually involved. In this Section we demonstrate the practical realization of this concept based on an experimental scheme with two pump pulses.

A. Double-pump coherent magnetization control via the inverse Faraday effect

For this optomagnetic mechanism, ultrafast coherent control of the magnetization can be very easily demonstrated by using multiple laser pulses in rapid succession. In a double pump experiment employing two circularly polarized pump pulses with opposite helicity and almost equal power, we achieved stopping of the precessional dynamics as well as doubling of the amplitude. Here and in the case of linearly polarized pulses below, we operate at a fixed time delay between the two pump pulses, and adjust the frequency of precession by an external magnetic field in order to vary the arrival time of the second pump pulse with respect to the phase of the precession already present.

In Fig. 23 it is shown how a pump pulse of helicity σ^+ arriving at $t=0$ triggers precession of the magnetization, as explained in the previous Section. A second pump pulse of helicity σ^- arriving after an odd number of half precessional periods rotates the magnetization further away from $\mathbf{H}_{\text{eff}}$, causing the subsequent precession to have almost twice the amplitude. If, however, this second pump pulse arrives after an integer number of full periods, the magnetization is rotated back into its original equilibrium orientation along $\mathbf{H}_{\text{eff}}$, and no further precession takes place. Figure 24 gives a pictorial illustration of these two situations.

This experiment clearly demonstrates that femtosecond optical pulses can be used to control spin dynamics directly and coherently. Depending on the phase of the precession when the second pulse arrives, energy is either transferred from the laser pulse to the magnetic system (amplification of the precession) or from the magnetic excitation to the optical pulse (stopping of the precession). A stimulated Raman process of scattering on magnons is believed to be responsible for the inverse Faraday effect[81] (see above), and we expect that further support for this mechanism can be found in the frequency spectrum of the second pump pulse. Stokes or anti-Stokes peaks should be observable in the spectrum, depending on whether the precession is amplified or stopped, respectively. In view of the low intrinsic damping in these garnet films, and therefore the long lifetime of magnetic excitations, it is remarkable how ultrashort laser pulses can

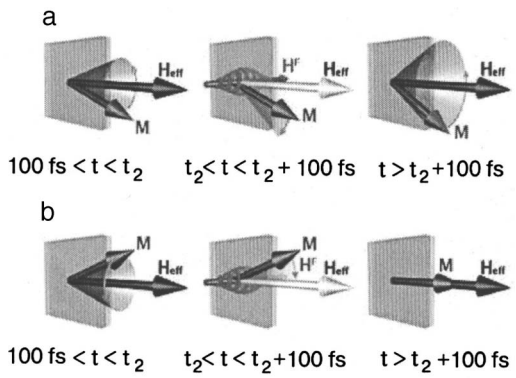

FIG. 24. Illustration of the double-pump experiment for circularly polarized pump pulses of opposite helicity arriving at (a) an odd number of half precessional periods and (b) an integer number of full precessional periods. The magnetization is either rotated further away from the effective field direction causing subsequent precession to take place with almost twice the original amplitude, or the magnetization is rotated back into the effective field direction and no further precession takes place.

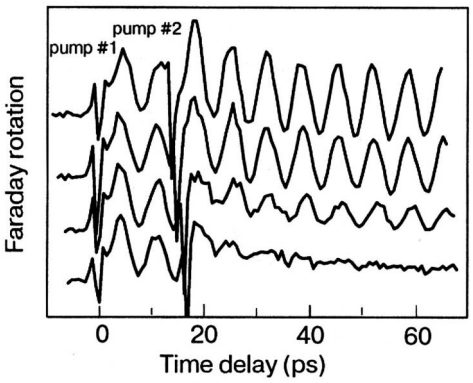

FIG. 25. Direct optical control of the magnetization dynamics in the dysprosium orthoferrite sample by two circularly polarized pump pulses of the same helicity. Depending on the time of arrival of the second pump pulse, the precession can be amplified or stopped completely.

completely stop the long-period coherent precession of spins instantaneously by transfer of the energy into the optical pulse. This process can also be viewed as coherent laser cooling of magnons.

In order to demonstrate the actual ultrafast magnetization control with inverse Faraday effect, we should turn our attention to experiments in antiferromagnetic orthoferrites, with characteristic precession periods of a few picoseconds. In Fig. 25 it is shown how two pump pulses, separated in time by about 16–18 ps, can be used to trigger and control the precession of **M**. By carefully timing the arrival of the second pump pulse, amplification as well as complete stopping of the precession can be achieved. This is the best demonstration so far of the unsurpassed speed with which magnetization control can be achieved using laser techniques. Strikingly, a change in the arrival time of the second pump pulse by only about a picosecond decides whether the system will be left in a stable state (lower curve) or with a large precession amplitude (upper curves). No existing electronics can even remotely approach these time scales.

It should be pointed out that the present double-pump experiments demonstrating control of the magnetization in ferrimagnetic garnets and antiferromagnetic orthoferrites are considerably different from those reported previously in diamagnetic and paramagnetic materials. During the past two decades a great number of publications have been devoted to the photoexcitation of a nonequilibrium spin polarization in direct bandgap semiconductors through the phenomenon of optical orientation.[101–103] In these materials, absorption of circularly polarized photons may lead to a nonequilibrium population of spin-polarized electrons and holes in the conduction band and valence band, respectively. In paramagnetic semiconductors these spin-polarized carriers can cause partial alignment of the moments of magnetic ions due to an *sp-d* exchange interaction and thereby also affect their precession in a magnetic field.[104] Using this phenomenon of optical orientation, Akimoto *et al.*[106] have demonstrated control of the precession of Mn^{2+} moments in $CdTe/Cd_{1-x}Mn_xTe$ quantum wells. Note that this approach, in contrast to our experiment, is based on the absorption of photons. A nonabsorptive mechanism for manipulation of spins in $Zn_{1-x}Cd_xSe$ quantum well structures was reported by Gupta *et al.*,[106] who used below-bandgap optical pulses to

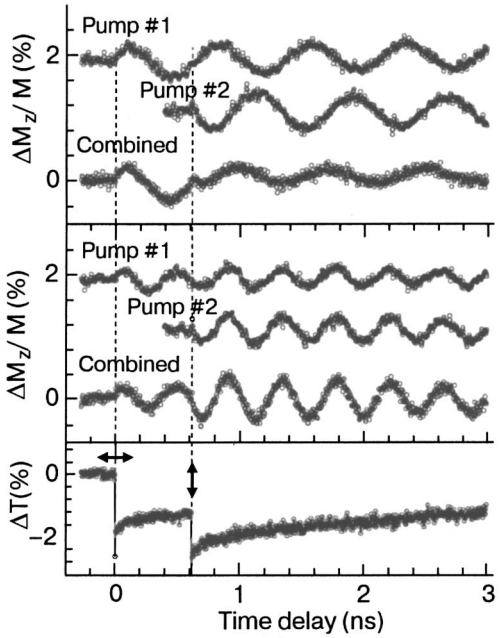

FIG. 26. A double-pump experiment with two 6-μJ orthogonal linearly polarized pump pulses separated in time by approximately 600 ps. Timing with respect to the spin precession is done by varying the in-plane applied magnetic field and thereby the precession frequency. The bottom panel shows the photoinduced change of sample transmissivity. Partial quenching (top panel) and amplification (middle panel) of the precession was achieved.[51]

control the spin precession of photoexcited electrons in the conduction band via the optical Stark effect. However, these experiments were performed on paramagnetic materials, while in the present case we have succeeded to control the collective motion of the strongly coupled spins in a magnetically ordered compound. Additionally, the experimental conditions differ strongly in the two cases; control of the spin precession in paramagnetic semiconductors requires very low temperatures, typically below 10 K, and strong magnetic fields of several tesla. In contrast, the optical control of magnetization that we report here was done at room temperature and in magnetic fields well below 1 kOe.

B. Double-pump control of anisotropy

In order to investigate the possibility of coherently modifying and controlling also the effective anisotropy fields on a time scale shorter than their relaxation time, a double-pump experiment was conducted on the magnetic garnet samples. Using a Michelson interferometer-like configuration, the pump pulses were split into two with a beam-splitter cube, and one part was delayed with respect to the other. As before, a fixed time delay was used and the timing of the arrival of the second pump pulse with respect to the precessional dynamics was controlled by varying the precession frequency (applied field). By use of a quarter wave plate the linear polarization of the second pump pulse was set to be orthogonal with respect to the first one. A magnetic field was applied in the plane of the sample, and the dynamics triggered by the individual pump pulses was first recorded by blocking one of the pump pulses at a time. The results are shown in Fig. 26. The two orthogonally polarized pump pulses (denoted by pump #1 and pump #2) trigger precession with the same

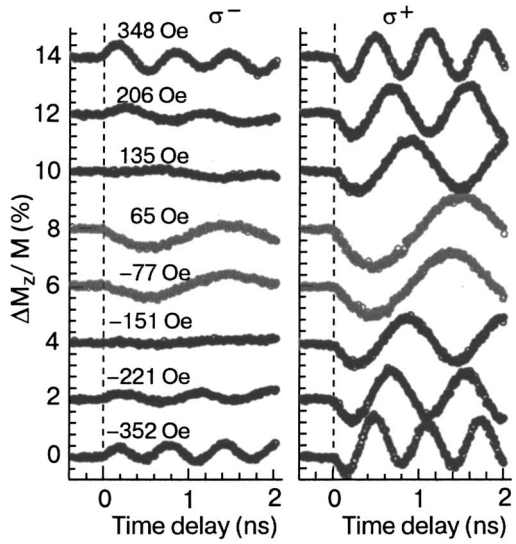

FIG. 27. Precession of the magnetization triggered by left- and right-circularly polarized laser pulses at different values of the in-plane applied magnetic field. For the σ^- helicity, at an applied field of $\sim\pm 150$ Oe, no precession is observed due to a perfect balance of the two photomagnetic effects $\delta\mathbf{H}^{an}$ and $\mathbf{H}^F$.

amplitude and opposite phase, a result which was also known from Fig. 17b. When allowing both pump pulses to reach the sample, the resulting dynamics (denoted combined) in the time after the second pump pulse ($t>0.6$ ns) is almost identical to the sum of the response of the two individual pump pulses. If the second pump pulse arrives after approximately one full precessional period, as shown in the top panel, it causes quenching of the subsequent dynamics. However, the timing was not accurate enough to completely quench the precession in the present case. If the second pump pulse arrives after one-and-a-half periods it causes subsequent precession with twice the amplitude, as shown in the middle panel. The two pump pulses appear to act completely independently, indicating that we are operating in the linear response regime (see Fig. 21). However, the experiment does not provide an answer to whether the long-lived anisotropy $\delta\mathbf{H}^{an}$ created by the first pump pulse is destroyed by the second pulse, or if the second pulse just creates additional anisotropy in the opposite direction.

C. Single-pump ultrafast photomagnetic switching

A proper combination of the inverse Faraday effect and the photoinduced anisotropy allows for an interesting demonstration of photomagnetic switching on a femtosecond time scale.[50] When the laser pulse is circularly polarized, the direction of $\delta\mathbf{H}^{an}$ depends only on the initial angle φ of the magnetization with respect to the crystal axes. Therefore, it can be tuned by rotating the sample with respect to the applied field. We have verified experimentally that this is the case. Alternatively, since the initial equilibrium of $\mathbf{H}_{eff}$, which is determined by the balance between the magnetocrystalline anisotropy field $\mathbf{H}_{an}$ and the externally applied field $\mathbf{H}_{ext}$, it can also be tuned simply by varying the strength of the applied field.

In Fig. 27 the coherent precession of the magnetization following excitation with pulses of helicity σ^- and σ^+ is shown for different values of $\mathbf{H}_{ext}$. The amplitude of precession is consistently larger in the case of σ^+, as during $0<t<100$ fs the $\mathbf{M}$ vector precesses away from the new equilibrium created by $\delta\mathbf{H}^{an}$, as explained above in Sec. IV B 2. For pulses of helicity σ^-, this precession is towards the new equilibrium, leading to smaller precessional amplitude in the time after the pulse. With an applied field of $|\mathbf{H}_{ext}|\approx 150$ Oe, no precession is triggered due to a perfect balance of two effects: The in-plane precession of the magnetization during the 100 fs magnetic field pulse $\delta\mathbf{H}^F$ brings the magnetization exactly to its new equilibrium orientation created by the optically modified anisotropy field. It remains stable in this orientation until the anisotropy field relaxes back to its original state, i.e., for several nanoseconds. An illustration of this switching process is shown in Fig. 28.

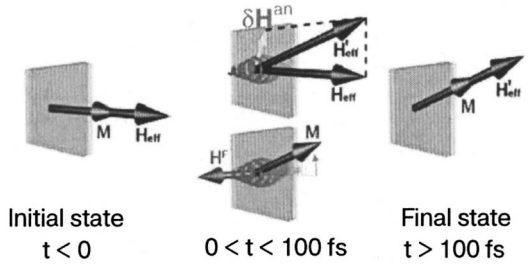

FIG. 28. Illustration of the switching process. Initially at $t<0$ the magnetization is along $\mathbf{H}_{eff}$. During the existence of the laser pulse $0<t<100$ fs photoinduced modification of the anisotropy fields leads to a new long-lived equilibrium along $\mathbf{H}'_{eff}$. Simultaneously, the strong optomagnetically generated field $\mathbf{H}^F$ causes the magnetization to precess into the new state. After $t>100$ fs the optical pulse is gone and the approximately 0.6° switching of $\mathbf{M}$ is complete.[51]

Note also that for the σ^- helicity at weak applied fields the precession has the opposite phase compared to the precession in stronger applied fields, and that this phase is the same as for the precession triggered by the σ^+ pulses. At weak fields the direction of the photoinduced $\delta\mathbf{H}^{an}$ is such that the precession of $\mathbf{M}$ in $\mathbf{H}^F$ during the optical pulse is not sufficient to bring it into the direction of $\mathbf{H}'_{eff}$. At stronger fields, however, $\delta\mathbf{H}^{an}$ is in a different direction producing an $\mathbf{H}'_{eff}$ that is less inclined with respect to the original effective field. During the existence of $\mathbf{H}^F$ the magnetization now precesses past the direction of $\mathbf{H}'_{eff}$, and therefore with the opposite phase in the time directly after the laser pulse.

VI. CONCLUSION

In this paper we have summarized our recent work on laser-induced magnetization dynamics in magnetic dielectrics. We have shown that in contrast to what was accepted earlier, such dynamics can occur at very short time scales. This happens due to the presence of strong photo- and optomagnetic effects in these materials. The latter are particularly interesting because optical absorption is not involved in the process. Instead, the effective mechanism is due to a Raman-like scattering process and, similar to the magnetooptical Faraday or Kerr effect, is described via the optical dispersion. From this, it may look like this "optomagnetism" is just an inverse form of the usual magnetooptics. This is partially true, as the two phenomena are described by the same material parameters.[77,78] The most important difference, however,

is that while the usual magnetooptic effects always serve as measurement tools, the inverse effects provide means for full control of the spin system.

We have started by elucidating thermal effects and have shown for the example of iron borate that heating of the spin system happens via phonon-magnon coupling. Although the latter was shown to be stronger than expected,[44] the characteristic relaxation time was still about 700 ps. Thus thermal interactions could be easily excluded in the treatment of the ultrafast nonthermal photo- and optomagnetic effects.

Using such effects, we have shown that the magnetization in garnet films and orthoferrite single crystals can be directly and coherently controlled on the femtosecond time scale with ultrashort laser pulses. Two distinct nonthermal effects that facilitate such control have been identified. A long-lived photomagnetically induced magnetic anisotropy field can be created by both linearly and circularly polarized laser pulses. In addition, strong transient magnetic field pulses can be generated by circularly polarized light via the optomagnetic inverse Faraday effect. Applying a small external field allows for the careful timing and balancing of these two effects, thus making complete nonthermal and coherent control of the magnetization possible. Moreover, by using multiple excitation pulses, either of these two effects can be used for a full coherent control of magnetic precession, with repetition frequencies of up to terahertz. Therefore the reported effects open up new and exciting possibilities for ultrafast manipulation of magnetization by light.

This work was supported by The Norwegian Research Council, The European RTN network DYNAMICS, Nederlandse Organisatie voor Wetenschappelijk Onderzoek (NWO), Stichting voor Fundamenteel Onderzoek der Materie (FOM), and the Russian Foundation for Basic Research (RFBR).

[a]E-mail: A.Kirilyuk@science.ru.nl

[1]A sharp step-like reduction of the magnetooptical signal within 1 ps occasionally observed, similar to that reported in Ref. 69. After additional experiments we concluded that in $FeBO_3$ this step-like behavior is an artifact related to the pump-induced transmissivity changes (Fig. 5a). By a proper calibration, the step-like contribution can be suppressed.

[1]E. Beaurepaire, J.-C. Merle, A. Daunois, and J.-Y. Bigot, Phys. Rev. Lett. **76**, 4250 (1996).
[2]C. H. Back, D. Weller, J. Heidmann, D. Mauri, D. Guarisco, E. L. Garwin, and H. C. Siegmann, Phys. Rev. Lett. **81**, 3251 (1998).
[3]C. H. Back, R. Allenspach, W. Weber, S. S. P. Parkin, D. Weller, E. L. Garwin, and H. C. Siegmann, Science **285**, 864 (1999).
[4]Y. Acremann, C. H. Back, M. Buess, O. Portmann, A. Vaterlaus, D. Pescia, and H. Melchior, Science **290**, 492 (2000).
[5]Y. Acremann, M. Buess, C. H. Back, M. Dumm, G. Bayreuther, and D. Pescia, Nature (London) **414**, 51 (2001).
[6]Th. Gerrits, H. A. M. van den Berg, J. Hohlfeld, L. Bar, and Th. Rasing, Nature (London) **418**, 509 (2002).
[7]C. Stamm, I. Tudosa, H. C. Siegmann, J. Stohr, G. Ju, B. Lu, and D. Weller, Nature (London) **428**, 831 (2004).
[8]C. Stamm, I. Tudosa, H. C. Siegmann, J. Stohr, A. Yu. Dobin, G. Woltersdorf, B. Heinrich, and A. Vaterlaus, Phys. Rev. Lett. **94**, 197603 (2005).
[9]A. V. Kimel, A. Kirilyuk, A. Tsvetkov, R. V. Pisarev, and Th. Rasing, Nature (London) **429**, 850 (2004).
[10]A. V. Kimel, A. Kirilyuk, P. A. Usachev, R. V. Pisarev, A. M. Balbashov, and Th. Rasing, Nature (London) **435**, 655 (2005).
[11]U. Keller, Nature (London) **424**, 831 (2003).
[12]M. B. Agranat, S. I. Ashitkov, A. B. Granovskii, and G. I. Rukman, Zh. Éksp. Teor. Fiz. **86**, 1376 (1984) [Sov. Phys. JETP **59**, 804 (1984)].
[13]A. Vaterlaus, T. Beutler, and F. Meier, J. Appl. Phys. **67**, 5661 (1990).
[14]A. Vaterlaus, T. Beutler, and F. Meier, Phys. Rev. Lett. **67**, 3314 (1991).
[15]A. Scholl, L. Baumgarten, R. Jacquemin, and W. Eberhardt, Phys. Rev. Lett. **79**, 5146 (1997).
[16]J. Hohlfeld, E. Matthias, R. Knorren, and K. H. Bennemann, Phys. Rev. Lett. **78**, 486 (1997).
[17]J. Güdde, U. Conrad, V. Jähnke, J. Hohlfeld, and E. Matthias, Phys. Rev. B **59**, R6608 (1999).
[18]E. Beaurepaire, M. Maret, V. Halté, J. C. Merle, A. Daunois, and J.-Y. Bigot, Phys. Rev. B **58**, 12134 (1998).
[19]H. Regensburger, R. Vollmer, and J. Kirschner, Phys. Rev. B **61**, 14716 (2000).
[20]B. Koopmans, M. van Kampen, J. T. Kohlhepp, and W. J. M. de Jonge, Phys. Rev. Lett. **85**, 844 (2000).
[21]P. M. Oppeneer and A. Liebsch, J. Phys.: Condens. Matter **16**, 5519 (2004).
[22]L. Guidoni, E. Beaurepaire, and J.-Y. Bigot, Phys. Rev. Lett. **89**, 017401 (2002).
[23]E. Beaurepaire, G. M. Turner, S. M. Harrel, M. C. Beard, J.-Y. Bigot, and C. A. Schmuttenmaer, Appl. Phys. Lett. **84**, 3465 (2004).
[24]J.-Y. Bigot, L. Guidoni, E. Beaurepaire, and P. N. Saeta, Phys. Rev. Lett. **93**, 077401 (2004).
[25]W. Hübner and G. P. Zhang, Phys. Rev. B **58**, R5920 (1998).
[26]A. Vernes and P. Weinberger, Phys. Rev. B **71**, 165108 (2005).
[27]G. Ju, A. V. Nurmikko, R. F. C. Farrow, R. F. Marks, M. J. Carey, and B. A. Gurney, Phys. Rev. Lett. **82**, 3705 (1999).
[28]G. Ju, L. Chen, A. V. Nurmikko, R. F. C. Farrow, R. F. Marks, M. J. Carey, and B. A. Gurney, Phys. Rev. B **62**, 1171 (2000).
[29]M. van Kampen, C. Jozsa, J. T. Kohlhepp, P. LeClair, L. Lagae, W. J. M. de Jonge, and B. Koopmans, Phys. Rev. Lett. **88**, 227201 (2002).
[30]Q. Zhang, A. V. Nurmikko, A. Anguelouch, G. Xiao, and A. Gupta, Phys. Rev. Lett. **89**, 177402 (2002).
[31]R. Wilks, R. J. Kicken, M. Ali, B. J. Hickey, J. D. R. Buchanan, A. T. G. Pym, and B. K. Tanner, J. Appl. Phys. **95**, 7441 (2004).
[32]M. Vomir, L. H. F. Andrade, L. Guidoni, E. Beaurepaire, and J.-Y. Bigot, Phys. Rev. Lett. **94**, 237601 (2005).
[33]G. P. Zhang and W. Hübner, Phys. Rev. Lett. **85**, 3025 (2000).
[34]G. Ju, A. Vertikov, A. V. Nurmikko, C. Canady, G. Xiao, R. F. C. Farrow, and A. Cebollada, Phys. Rev. B **57**, R700 (1998).
[35]J.-Y. Bigot, C. R. Acad. Sci. Ser. IV (Paris) **2**, 1483 (2001).
[36]Recently we have managed to suppress this dominating thermal effect in GdFeCo and to observe true nonthermal effects: C. D. Stanciu, F. Hansteen, A. V. Kimel, A. Tsukamoto, A. Itoh, A. Kirilyuk, and Th. Rasing, to be published.
[37]H. Ohno, Science **281**, 951 (1998).
[38]H. Ohno, A. Shen, F. Matsukura, A. Oiwa, A. Endo, S. Katsumoto, and Y. Iye, Appl. Phys. Lett. **69**, 363 (1996).
[39]A. Oiwa, Y. Mitsumori, R. Moriya, T. Slupinski, and H. Munekata, Phys. Rev. Lett. **88**, 137202 (2002).
[40]Y. Mitsumori, A. Oiwa, T. Slupinski, H. Maruki, Y. Kashimura, F. Minami, and H. Munekata, Phys. Rev. B **69**, 033203 (2004).
[41]A. V. Kimel, G. V. Astakhov, G. M. Schott, A. Kirilyuk, D. R. Yakovlev, G. Karczewski, W. Ossau, G. Schmidt, L. W. Molenkamp, and Th. Rasing, Phys. Rev. Lett. **92**, 237203 (2004).
[42]E. Kojima, R. Shimano, Y. Hashimoto, S. Katsumoto, Y. Iye, and M. Kuwata-Gonokami, Phys. Rev. B **68**, 193203 (2003).
[43]J. Wang, C. Sun, J. Kono, A. Oiwa, H. Munekata, L. Cywiński, and L. J. Sham, Phys. Rev. Lett. **95**, 167401 (2005).
[44]A. V. Kimel, R. V. Pisarev, J. Hohlfeld, and Th. Rasing, Phys. Rev. Lett. **89**, 287401 (2002).
[45]G. Winkler, *Magnetic Garnets*, Friedr. Vieweg & Sohn, Braunschweig, Germany (1981).
[46]A. Paoletti (ed.), *Physics of Magnetic Garnets*, Enrico Fermi International School of Physics, Italian Physical Society, North-Holland (1978).
[47]A. B. Chizhik, I. I. Davidenko, A. Maziewski, and A. Stupakiewicz, Phys. Rev. B **57**, 14366 (1998).
[48]A. Stupakiewicz, A. Maziewski, I. Davidenko, and V. Zablotskii, Phys. Rev. B **64**, 064405 (2001).
[49]A. F. Kabychenkov, Zh. Éksp. Teor. Fiz. **100**, 1219 (1991) [JETP **73**, 672 (1991)].
[50]F. Hansteen, A. V. Kimel, A. Kirilyuk, and Th. Rasing, Phys. Rev. Lett. **95**, 047402 (2005).
[51]F. Hansteen, A. V. Kimel, A. Kirilyuk, and Th. Rasing, Phys. Rev. B **73**, 014421 (2006).
[52]R. L. White, J. Appl. Phys. **40**, 1061 (1969).

[53]V. F. Kovalenko and E. L. Nagaev, Sov. Phys. Usp. **29**, 297 (1986).
[54]B. B. Krichevtsov, V. V. Pavlov, and R. V. Pisarev, JETP Lett. **49**, 466 (1989).
[55]R. V. Pisarev, B. B. Krichevtsov, V. N. Gridnev, V. P. Klin, D. Fröhlich, and C. Pahlke-Lerch, J. Phys.: Condens. Matter **5**, 8621 (1993).
[56]F. Hansteen, O. Hunderi, T. H. Johansen, A. Kirilyuk, and Th. Rasing, Phys. Rev. B **70**, 094408 (2004).
[57]*Numerical Data and Functional Relationships*, Landolt-Börnstein, New Series, Group III, Vol. 27 f, Springer-Verlag, Berlin (1981).
[58]I. E. Dzyaloshinskii, Sov. Phys. JETP **5**, 1259 (1957).
[59]T. Moriya, Phys. Rev. **120**, 91 (1960).
[60]A. K. Zvezdin and V. A. Kotov, *Modern Magnetooptics and Magnetooptical Materials*, IOP, Bristol (1997).
[61]A. M. Balbashov and S. K. Egorov, J. Cryst. Growth **52**, 498 (1981).
[62]K. P. Belov, R. A. Volkov, B. P. Goranskii, A. M. Kadomtseva, and V. V. Uskov, Fiz. Tverd. Tela (Leningrad) **11**, 1148 (1969) [Sov. Phys. Solid State **11**, 935 (1969)].
[63]P. A. Usachev, R. V. Pisarev, A. M. Balbashov, A. V. Kimel, A. Kirilyuk, and Th. Rasing, Phys. Solid State **47**, 2292 (2005).
[64]A. Tsukamoto, K. Nakagawa, A. Itoh, A. Kimel, A. Tsvetkov, H. A. N. Ohta, A. Kirilyuk, and Th. Rasing, IEEE Trans. Magn. **40**, 2543 (2004).
[65]L. Landau and E. Lifshitz, Phys. Z. Sowjetunion **8**, 153 (1935).
[66]B. Hillebrands and K. Ounadjela (eds.), *Spin Dynamics in Confined Magnetic Structures I*, Springer-Verlag, Berlin (2002).
[67]R. M. White, R. J. Nemanich, and C. Herring, Phys. Rev. B **25**, 1822 (1982).
[68]A. M. Balbashov, G. V. Kozlov, A. A. Mukhin, and A. S. Prokhorov, in *High Frequency Processes in Magnetic Materials*, G. Srinivasan and A. N. Slavin (eds.), World Scientific, Singapore (1995), p. 56.
[69]T. Kise, T. Ogasawara, M. Ashida, Y. Tomioka, Y. Tokura, and M. Kuwata-Gonokami, Phys. Rev. Lett. **85**, 1986 (2000).
[70]L. D. Landau and E. M. Lifshitz, *Electrodynamics of Continuous Media*, Pergamon, Oxford (1960).
[71]A. B. P. Lever, Inorganic Electronic Spectroscopy, Elsevier Science, Amsterdam (1984).
[72]Y. Tanabe and K. Aoyagi, in *Excitons*, Vol. 2, E. I. Rashba and M. D. Sturge (eds.), North-Holland, Amsterdam (1982).
[73]C. Kittel, Phys. Rev. **110**, 836 (1958).
[74]A. I. Akhiezer, V. G. Bar'yakhtar, and S. V. Peletminskii, *Spin Waves*, North-Holland, Amsterdam (1968).
[75]O. S. Kolotov, A. P. Krasnozhon, and V. A. Pogozhev, Phys. Solid State **38**, 565 (1996).
[76]L. P. Pitaevskii, Sov. Phys. JETP **12**, 1008 (1961).
[77]P. S. Pershan, J. P. van der Ziel, and L. D. Malmstrom, Phys. Rev. **143**, 574 (1966).
[78]J. P. van der Ziel, P. S. Pershan, and L. D. Malmstrom, Phys. Rev. Lett. **15**, 190 (1965).
[79]C. Kittel, Phys. Rev. **73**, 155 (1948).
[80]R. R. Birss, *Symmetry and Magnetism*, Series of Monographs on Selected Topics in Solid State Physics, North-Holland Publishing Company (1966).
[81]Y. R. Shen and N. Bloembergen, Phys. Rev. **143**, 372 (1966).
[82]R. Gómez-Abal, O. Ney, K. Satitkovitchai, and W. Hübner, Phys. Rev. Lett. **92**, 227402 (2004).
[83]A. M. Balbashov, A. A. Volkov, S. P. Lebedev, A. A. Mukhin, and A. S. Prokhorov, Sov. Phys. JETP **61**, 573 (1985).
[84]N. Koshizuka and K. Hayashi, J. Phys. Soc. Jpn. **57**, 4418 (1988).
[85]H. Horner and C. M. Varma, Phys. Rev. Lett. **20**, 845 (1968).
[86]S. M. Shapiro, J. D. Axe, and J. P. Remeika, Phys. Rev. B **10**, 2014 (1974).
[87]Koster, J. O. Dimmock, R. G. Wheeler, and H. Statz, *Properties of the Thirty-Two Point Groups*, MIT Press, Cambridge, MA (1963).
[88]L. D. Landau and E. M. Lifshitz, Phys. Z. Sowjetunion **8**, 153 (1935).
[89]H. W. Schumacher, C. Chappert, P. Crozat, R. C. Sousa, P. P. Freitas, J. Miltat, J. Fassbender, and B. Hillebrands, Phys. Rev. Lett. **90**, 017201 (2003).
[90]V. Skumryev, S. Stoyanov, Y. Zhang, G. Hadjipanayis, D. Givord, and J. Nogués, Nature (London) **423**, 850 (2003).
[91]Y. R. Shen, *The Principles of Nonlinear Optics*, Wiley, New York (1984).
[92]T. H. O'Dell, *The Electrodynamics of Magneto-Electric Media*, North-Holland, Amsterdam (1970).
[93]V. V. Pavlov, R. V. Pisarev, A. Kirilyuk, and Th. Rasing, Phys. Rev. Lett. **78**, 2004 (1997).
[94]R. W. Teale and D. W. Temple, Phys. Rev. Lett. **19**, 904 (1967).
[95]J. F. Dillon, E. M. Gyorgy, and J. P. Remeika, Phys. Rev. Lett. **22**, 643 (1969).
[96]R. Alben, E. M. Gyorgy, J. F. Dillon, and J. P. Remeika, Phys. Rev. B **5**, 2560 (1972).
[97]V. G. Veselago, R. A. Doroshenko, and S. G. Rudov, Zh. Éksp. Teor. Fiz. **105**, 638 (1994) [JETP **78**, 341 (1994)].
[98]R. Metselaar, M. A. H. Huyberts, and H. Logmans, J. Appl. Phys. **46**, 7326 (1975).
[99]V. V. Eremenko, S. L. Gnatchenko, I. S. Kachur, V. G. Piryatinskaya, A. M. Ratner, and V. V. Shapiro, Phys. Rev. B **61**, 10670 (2000).
[100]N. P. Duong, T. Satoh, and M. Fiebig, Phys. Rev. Lett. **93**, 117402 (2004).
[101]F. Meier and B. P. Zakharchenya (eds.), *Optical Orientation*, Vol. 8 of Modern Problems in Condensed Matter Sciences, North-Holland, Amsterdam (1984), ISBN 0-444-86741-4.
[102]D. D. Awschalom, J. Warnock, and S. von Molnár, Phys. Rev. Lett. **58**, 812 (1987).
[103]I. Zutic, J. Fabian, and S. Das Sarma, Rev. Mod. Phys. **76**, 323 (2004).
[104]J. K. Furdyna and J. Kossut (eds.), *Diluted Magnetic Semiconductors*, Vol. 25 of Semiconductors and Semimetals, Academic Press, New York (1988), ISBN 0-12-752125-9.
[105]R. Akimoto, K. Ando, F. Sasaki, S. Kobayashi, and T. Tani, J. Appl. Phys. **84**, 6318 (1998).
[106]J. A. Gupta, R. Knobel, N. Samarth, and D. D. Awschalom, Science **292**, 2458 (2001).

This article was published in English in the original Russian journal. Reproduced here with stylistic changes by AIP.